The Roles of Antecedent Soil Moisture and Land-Atmosphere Interactions in the Inland Intensification of Tropical Storm Bill (2015)

Jinwoong Yoo[1, 2], Joseph A. Santanello, Jr.[1], Patricia Lawston-Parker[1, 2], J. Marshall Shepherd[3], Sujay V. Kumar[1], and Ryann Wakefield[4]

[1]NASA Goddard Space Flight Center,

[2]University of Maryland (ESSIC),

[3]University of Georgia,

[4]National Grid

Corresponding Author: Dr. Jinwoong Yoo

NASA-GSFC, Code 617, Bldg. 33, Room G218, Greenbelt, MD 20771 USA

Jinwoong.yoo@nasa.gov

Submitted to *Journal of Hydrometeorology*

Abstract

Extreme weather events cause significant societal impacts, in particular, when they behave unexpectedly. The 'Brown Ocean (BO)' effect, describing the ability of the land surface via soil moisture to support tropical cyclone (TC) maintenance and intensification (TCMI) after landfall, remains poorly understood. Building upon our previous modeling framework utilizing the NASA Unified WRF (NU-WRF) system, this follow-on study explores the contributions of the dynamics of the soil moisture and advected water vapor to the TCMI of TS Bill (2015) over the U.S. Southern Great Plain (SGP). Impacts of various soil moisture conditions and surface enthalpy flux conditions on Bill's inland intensification were investigated by comparing their land-atmosphere interaction components of energy fluxes along with a backward trajectory analysis and three-dimensional visualization of low-level atmospheric moisture. Results demonstrate that the high antecedent soil moisture across the Central U.S. (Great Plains and Mississippi Valley) from prior rainfall was crucial for the TCMI of TS Bill over the SGP. Without ample latent heat flux over land, even a moisture-laden low-level jet from the ocean rapidly dried over land, preventing intensification and causing storm dissipation in our simulations. Backward trajectory analysis suggests that high soil moisture content can enhance humidity within the storm's inflow, including the advection from the ocean, far inland, thus supporting TCMIs. Ultimately, the inflow feeding the inland TC core is influenced by active land-air interactions within the boundary layer, where soil moisture and lower boundary conditions directly impact lower tropospheric humidity, enabling or hindering the BO effect and subsequent TC intensification.

Keywords: Brown ocean effect, TCMI, landfalling tropical cyclone, soil moisture, land-atmosphere interactions, inflow trajectory analysis.

1. Introduction

Extreme weather events, such as tropical cyclones (TCs) can have a large impact on society, in part, because they are poorly understood and a challenge to predict. Even with advanced satellite observations and numerical weather forecasting skill, predicting TC intensity remains a challenging task for weather forecasting agencies, leaving TCs as one of the most-deadly extreme weather events globally. Moreover, rapid intensifications of TCs near shore or sudden reintensification of TCs post-landfall often impose great anxiety on entire coastal societies in the Northern Gulf of Mexico including Houston, New Orleans, and Mobile. Also note that most of the US landfalling storms tend to move towards densely populated regions along the Eastern seaboard.

Hall and Kossin (2019) found a significant positive trend in coastal annual-mean rainfall 1948–2017 from TCs that stall, which is associated with increased frequency of slow-moving storms. The 2021 Atlantic hurricane season, while not as record-breaking as 2020, was still above average and featured three notable storms: Claudette, Elsa, and Ida. These storms caused significant damage and loss of life due to their unusual behavior and intensity, particularly after making landfall. Tropical Storm Claudette intensified rapidly upon landfall (https://www.weather.gov/mob/claudette), Hurricane Elsa transitioned to an extratropical storm causing widespread flooding (https://www.weather.gov/tbw/HurricaneElsa), and Hurricane Ida, reminiscent of Katrina, devastated both the Gulf Coast and the Northeast with tornadoes and catastrophic flooding (https://www.weather.gov/lch/2021Ida). These events underscore the need for improved understanding and prediction of TC intensification over land, particularly the influence of land-atmosphere interactions and soil moisture.

From a statistical point of view, tropical cyclogenesis (TCG) is a very rare event among the numerous mesoscale convective systems (MCSs) continuously existing in the tropical or subtropical oceans globally. In the North Atlantic, only about ten tropical storms and five to six hurricanes develop from one hundred tropical disturbances in a typical year. As such, a tiny fraction of the MCSs develop into tropical cyclones (TCs), and only when specific set of geophysical constraints and conditions in multi-scales are met, including warm sea surface temperatures, pre-existing atmospheric turbulence with low-level relative vorticity, relatively weak wind shear between lower and upper troposphere, high mid-troposphere relative humidity,

and the vertical gradient of potential temperature between the sea surface and 500 hPa level of atmosphere (Gray, 1975). Once the "heat engine" of a TC (Emanuel, 1986) is established, it runs as long as the supply of the enthalpy from the surface (i.e., ocean in general) can produce enough latent heat released for the TC warm core in the atmosphere via the phase changes of atmospheric water (e.g., condensation, freezing, and/or sublimation). If the condition of the barotropic atmosphere environment of the TC is consistent, the sustainability of the TC heat engine is, therefore, primarily dependent on the availability of the surface enthalpy in the TC core regardless of whether the TC is located over the ocean or the land. Hence, TCs often pass over coastal terrain or peninsulas, and continue their track without greatly diminishing their intensity or their TC circulation patterns (e.g., Hurricanes Katrina and Wilma in 2005; Figure A1).

Theoretically, the same physical mechanism should be valid even when a TC moves over land if their barotropic atmosphere features are retained after landfall. Amongst the TC community, the general consensus has traditionally been that the surface sensible and latent heat fluxes over land cannot sustain the warm core (i.e., heat engine) once the center of the circulation moves over the relatively dry land in contrast to over the ocean surface (Miller 1964; Ooyama 1969; Rosenthal 1971; Tuleya et al. 1984; Tuleya 1994; Kaplan and DeMaria 1995). However, changes in the general consensus started to form over the last decade as ample observations were made to suggest that TCs had survived after landfall quite a longer period of time than expected (e.g., 24 hours) maintaining or increasing their intensity (i.e., TCMIs; Emanuel et al. 2008; Andersen and Shepherd 2013). These TCs did not interact with the midlatitude baroclinic environment which is a typical intensification mechanism of extratropical cyclones (a.k.a., extratropical transition) (Hart and Evans 2001; Evans et al. 2011).

Consequently, physical mechanisms of TCMI events have been investigated by groups in the context of the Brown Ocean (BO) Effect (e.g., Andersen and Shepherd 2013). Nair et al. (2019) provided an analysis of an unusual tropical low that intensified over the coastal terrain of Louisiana and caused severe flooding in Baton Rouge, Louisiana in 2016. Although the intensification of the tropical low was in part associated with the moisture advection from the Gulf of Mexico due to the storm's proximity to the coastline, they showed that land cover and soil moisture conditions in the vicinity of the storm played a critical role in the reintensification

of the tropical low over land. Yoo et al. (2020) followed by establishing a numerical model simulation framework to test the impacts of the land surface fluxes on the TCMI of Tropical Cyclone Kelvin (2018) in Australia using the NASA Unified Weather Research and Forecasting (NU-WRF; Peters-Lidard *et al*. 2015). In particular, they suggested a clear methodology to quantitatively analyze the role of the soil moisture in the reintensification of the TC post-landfall by controlling the surface evaporation through varying soil moisture initialization using the NASA Land Information System (LIS; Kumar et al. 2006; Peters-Lidard et al. 2007). TC Kelvin's reintensification over land was dominated by the moisture advection from the tropical ocean (i.e., intertropical convergence zone) to the north of the landfall region. In fact, this result of the study by Yoo et al. (2020) adjusted the perspectives of the BO Effect in which the impacts of the land surface fluxes on TCMIs act on a continuum rather than the binary (i.e., all or nothing). Wakefield et al. (2021) provided a consolidated set of data that shows the TCMI of Tropical Storm (TS) Bill (2015) post-landfall could be differentiated from those of non-TCMI storms, which is also supportive of the BO Effect. By analyzing polarimetric radar signatures, the studies of Brauer et al. (2021) showed that the TS Bill maintained tropical characteristics of warm rain during its multiple TCMI periods over land. Furthermore, Zhu et al. (2022) suggested that increased soil moisture due to preceding precipitation was associated with the slow weakening rate of the Hurricane Ida (2021) post landfall. Using both satellite observations of soil moisture and model simulations, Li et al. (2023) related the BO Effect of wet and warm antecedent soil moisture with rainfall intensity during Hurricane Florence (2018).

While previous studies have explored the influence of soil moisture on Tropical Cyclone Maintenance and Intensification (TCMI) through limited sensitivity analyses, they lacked a comprehensive understanding of the underlying processes. Building on the previous BOE studies, this study aims to address this gap by investigating the complex interplay between local and non-local effects of surface enthalpy fluxes and their transport along air parcel trajectories within the TC inflow environment over the ocean-land transition zone. Specifically, this research will elucidate the impact of soil moisture on the key mechanisms of the BO effect, as demonstrated by Tropical Storm Bill, a phenomenon not fully explored in previous studies. The inland reintensification of Tropical Storm Bill, along with that of Tropical Storm Erin in 2007, garnered significant attention in both media and research (e.g., Wakefield et al. 2021 and references therein) due to the growing interest in the BO effect sparked by Andersen and

Shepherd's seminal 2013 work. The selection of Tropical Storm Bill for this study was motivated by previous observational studies suggesting that its maintenance of barotropic characteristics during Tropical Cyclone Maintenance and Intensification (TCMI) aligns with the hypothetical requirements of a BO effect storm. Overall, building upon the numerical model simulation framework developed by Yoo et al. (2020), we hypothesize that variations in soil moisture (e.g., wet vs. dry) and the resulting differences in surface enthalpy fluxes across the coastal and inland regions within the TC inflow will significantly impact the energy and moisture characteristics of inflowing air parcels, ultimately influencing the TCMI of the inland storm. Furthermore, we hypothesize that a TC center-following back trajectory analysis will elucidate the TC inflow dynamics after landfall, revealing differences compared to those of a TC over the ocean.

2. Data and Methods

2.1. Model and Experiment Design

This study utilizes the modeling framework of Yoo et al. (2020) to investigate the TCMI process mechanisms of TS Bill (2015) by deploying a set of permutations of land-atmosphere coupled simulations using the NU-WRF model. The NU-WRF model is a regional earth system modeling and data assimilation system that operates at satellite-resolvable scales and is driven by observations. It is based on the Advanced Research WRF (ARW) developed by NCAR, but incorporates NASA's advanced physics modules, satellite simulators, and ensemble data assimilation system, as well as the NASA LIS. NU-WRF has been used to study a range of earth science phenomena, such as aerosol (e.g., Shi et al. 2021; Tao et al. 2020), cloud (e.g., Tao et al. 2018), precipitation (e.g., Kim et al. 2018), and land processes, and their interactions (e.g., Santanello et al. 2019). In particular, LIS plays a critical role in the study of L-A interactions by providing a better informed land surface temperature and moisture conditions via the spinup of the land surface models prior to the time of the initialization of the coupled simulation (Lawston et al. 2020, Santanello et al. 2016, 2019). We are leveraging these advantages of LIS model spinups within NU-WRF model simulations of the landfalling tropical cyclone for the improved and realistic representations of the soil conditions in initialization of the coupled model.

NU-WRF modeling experiments consist of three steps: land surface model spinup using LIS, pilot runs, and NU-WRF coupled simulations (i.e., LIS-WRF online coupled simulations). LIS spinup is to construct the abnormally wet soil moisture conditions due to precipitation in the

148 preceding months as well as realistic soil temperature conditions before TS Bill in 2015. To
149 assess the sensitivity to meteorological forcing data, two initial LIS spinups are driven by two
150 met-forcing datasets of Global Data Assimilation System (GDAS;
151 https://www.ncei.noaa.gov/products/weather-climate-models/global-data-assimilation) and North
152 American Land Data Assimilation version 2 (NLDAS2; https://ldas.gsfc.nasa.gov/nldas) using
153 Noah land surface model (v3.6) for more than five years (which is an empirical number of
154 spinup period) from the time stamp of 1 January 00 UTC, 2010 to 16 June 00 UTC, 2015. Then,
155 an additional LIS spinup is conducted using Noah-MP (v3.6) land surface model with the GDAS
156 forcing. Figure A2 shows the temporal evolutions of domain average soil moisture and
157 temperature of the spinup runs (i.e., Control (GDAS), NLDAS2, and NoahMP). The LIS spinup
158 results were comparable to each other in both soil moisture and temperature, particularly near the
159 time of the NU-WRF initialization. Therefore, the LIS spinup with NLDAS2 forcing using Noah
160 land surface model (LSM) was selected as the default LSM spinup case for the next step.
161 With the default LIS spinup case selected, the pilot runs are conducted to test the hindcast
162 performance with atmospheric forcing datasets and model physics as well as LIS spinup for the
163 WRF 3-dimensional atmospheric model before we select the "best" model configurations for the
164 NU-WRF simulations of TS Bill, as follows: 1) National Centers for Environmental Prediction
165 (NCEP) FNL (Final) data vs. European Centre for Medium-Range Weather Forecasts (ECMWF)
166 ERA5 (Dee et al. 2011) for atmospheric forcing, 2) NU-WRF physics options vs. NCAR WRF
167 Tropic physics options, and 3) LIS spinup vs. the intrinsic soil conditions of FNL and ERA5
168 datasets. The pilot runs include six model configurations cases named as gdas, gdas_nldas2,
169 gdas_noLIS, gdas_tropic, era5_noLIS, and era5_tropic (Table 1). Remotely sensed sea surface
170 temperature (SSTRSS) data are ingested every 6 hours during the five-day simulation of all the
171 pilot runs.
172
173 Table 1. Forcings and physics configurations of pilot run cases.
174

Pilot runs	Atm. forcing	LIS spinup	LSM forcing	Physics package
gdas	GDAS FNL	Yes	GDAS	NU-WRF physics
gdas_nldas2	GDAS FNL	Yes	NLDAS2	NU-WRF physics
gdas_noLIS	GDAS FNL	No	N/A	NU-WRF physics
gdas_tropic	GDAS FNL	No	N/A	WRF Tropical
era5_noLIS	ECMWF ERA5	No	N/A	NU-WRF physics
era5_tropic	ECMWF ERA5	No	N/A	WRF Tropical

The performance of the pilot WRF simulations is evaluated by their TC intensity hindcast against the TC Best Track records (i.e., IBTrACS; Knapp et al. 2010) of maximum sustained wind speed and minimum sea level pressure. Figure 1 shows the soil moisture distribution at the initial time of the pilot runs along with simulated storm's track and the Best Track. The initial soil moisture conditions in the ERA5 (Fig. 1a and b) were relatively higher than those by GDAS FNL (Fig. 1c and d) and by LIS spinups (Fig. 1e and f), which resulted in much slower TC translation speeds over the landfalling coast area, causing large errors both in TC track and intensity. It is conjectured that higher surface enthalpy from the wetter soil conditions in the ERA5 cases was associated with the much slower TC translation speeds as TCs slow down over a warmer sea surface area over the ocean in general. In contrast, the other pilot cases demonstrated relatively good performance in TC track hindcast. However, the gdas_tropic produced a much weaker storm compared to those with NU-WRF physics suite. The gdas_noLIS resulted in a slightly larger track error with an increased uncertainty with locating center of the storm toward the end of the TC simulation than the cases of gdas and gdas_nldas2, both of which performed best amongst the pilot runs in reproducing the TS Bill's track and intensity. From these results, the gdas case initialized by LIS spinup with GDAS forcing using Noah3.6 LSM (Fig. 1e) is selected as the Control simulation in our NU-WRF main simulation experiment. This decision is reflecting the fact that meteorological forcing with the GDAS dataset is considered as a "general" option while the NLDAS-2 is a dataset of "choice" with the highest resolution forcing with gauge-corrected precipitation. Therefore, we employ the two meteorological forcing options both in the pilot runs and the NU-WRF coupled runs to compare the model sensitivities in the TCMI experiments.

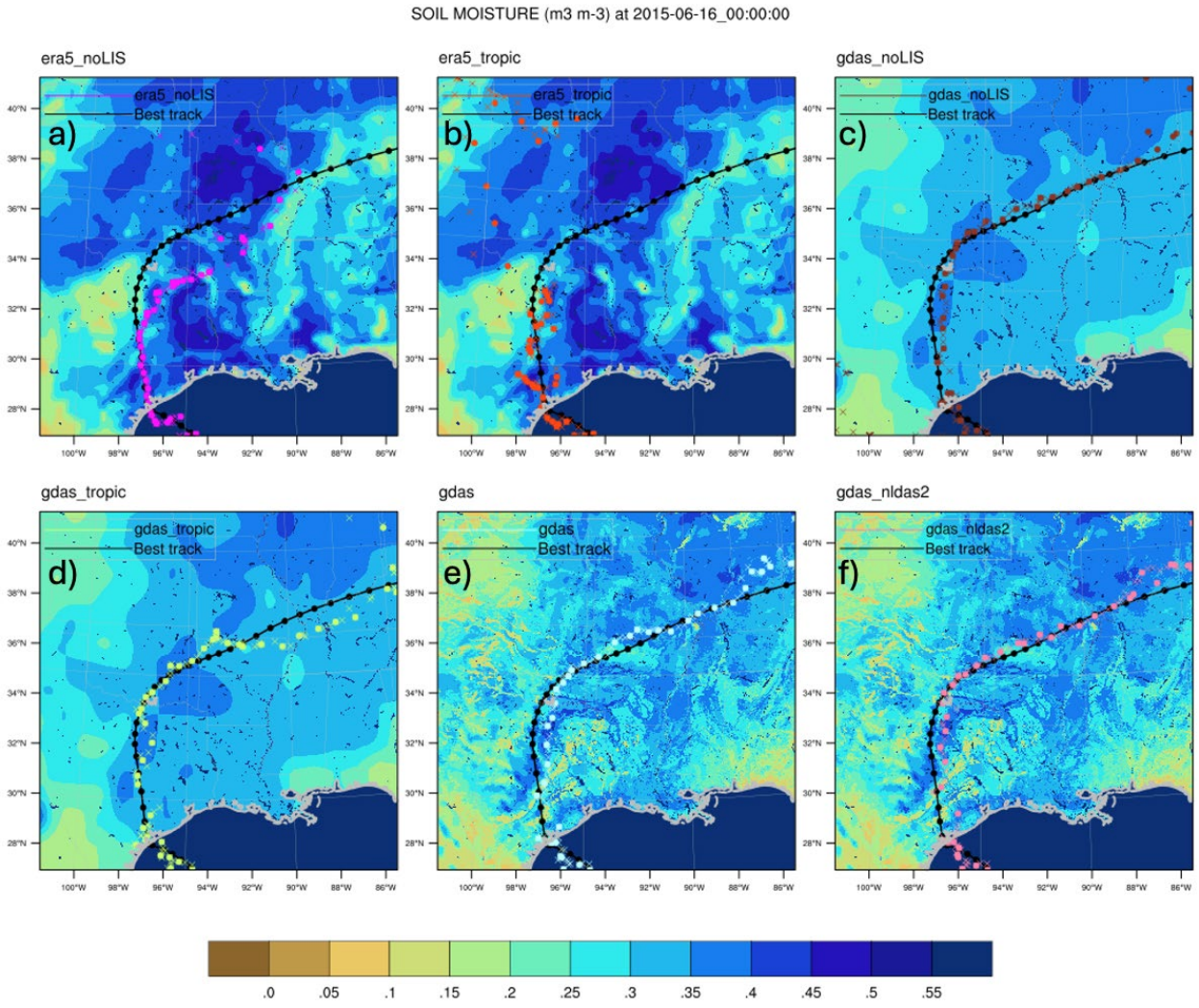

Figure 1. Initial soil moisture distribution at the top level of soil layers (centered at 5 cm) of the pilot runs with simulated storm's track and the Best track.

Having selected the control run, we perturb seven members of the NU-WRF simulations to consider the impacts of soil moisture conditions (Figure 2), PBL schemes, atmospheric forcing, and LSM selection on the TCMI of TS Bill. The seven permutations include cases of the control run (i.e., Control), Dry, NoLHF, Saturate, YSU, NLDAS2, and NoahMP (Table 2). Dry case is identical to the Control case but the fact that the initial soil moisture for the coupled land-atmosphere simulation is replaced by the driest domain averaged soil moisture condition during the LIS spinup (i.e., as on 2010-10-18) (Fig. 2b). The Dry case is intended to test how a naturally (horizontally and vertically) dry soil moisture distribution condition, in contrast to a completely dry soil with uniform wilting point values, will impact TCMI compared to the relatively high soil

moisture condition of the Control case. The NoLHF case is designed as such that LHF over the land in the Control case is completely suppressed (prescribed as zero at every time step) in the land surface model. Thus, the atmospheric model of WRF does not receive any LHF from the surface via the LSM [Note that the LSM behaves as usual in its simulation, and the land surface energy balance is therefore not closed, and represents an extreme unphysical state to amplify the impact of LHF.] and the landfalling storm does not receive any LHF from the land while it can take LHF from water bodies or from the ocean. This NoLHF case thereby isolates the impact of land evaporation contribution completely in the landfalling TC simulation when compared to the Control run. In contrast, the Saturate case is similar to the Control case of high soil moisture but its soil moisture is prescribed to the maximum capacity of the soil texture type (a.k.a. field capacity) at each grid cell within the domain throughout the simulation period (Fig. 2c). This Saturate case demonstrates the landfalling TC's response to the near-flooded soil moisture conditions. In addition, while not directly to quantify soil moisture effect, we included YSU, NLDAS2, and NoahMP experiments to understanding the sensitivity of the simulations and of the TCMI behavior to model physics (PBL, NoahMP) and LSM forcing *relative* to that of soil moisture for a broader purpose of the study, which was the goal of this ensemble of simulations. YSU case is also the same as the Control but YSU planetary boundary layer (PBL) scheme is applied instead of the MYNN PBL scheme in the Control case. NLDAS2 case is WRF model online coupled with LIS which is forced by North American Land Data Assimilation System version 2 (NLDAS2) dataset in 1/8th degree grid spacing resolution compared to the GDAS in control case. Finally, NoahMP case is the same as the Control but NoahMP3.6 LSM is applied.

Table 2. Modeling permutations with soil moisture conditions and other variations

Cases	**Soil Moisture State**	**PBL Opt.**	**3D Atm. /LSM forcing**	**LSM**
Control	**Wet (w/ LIS Spinup)**	MYNN	FNL/GDAS	Noah3.6
Dry	**Driest during LIS spinup**	MYNN	FNL/GDAS	Noah3.6
Saturate	**Saturated to field capacity by soil type**	MYNN	FNL/GDAS	Noah3.6
NoLHF	**No Latent Heat Flux from Land**	MYNN	FNL/GDAS	Noah3.6
YSU	Wet (w/ LIS Spinup)	**YSU**	FNL/GDAS	Noah3.6
NLDAS-2	Wet (w/ LIS Spinup)	MYNN	**FNL/NLDAS-2**	Noah3.6
NoahMP	Wet (w/ LIS Spinup)	MYNN	FNL/GDAS	**NoahMP**

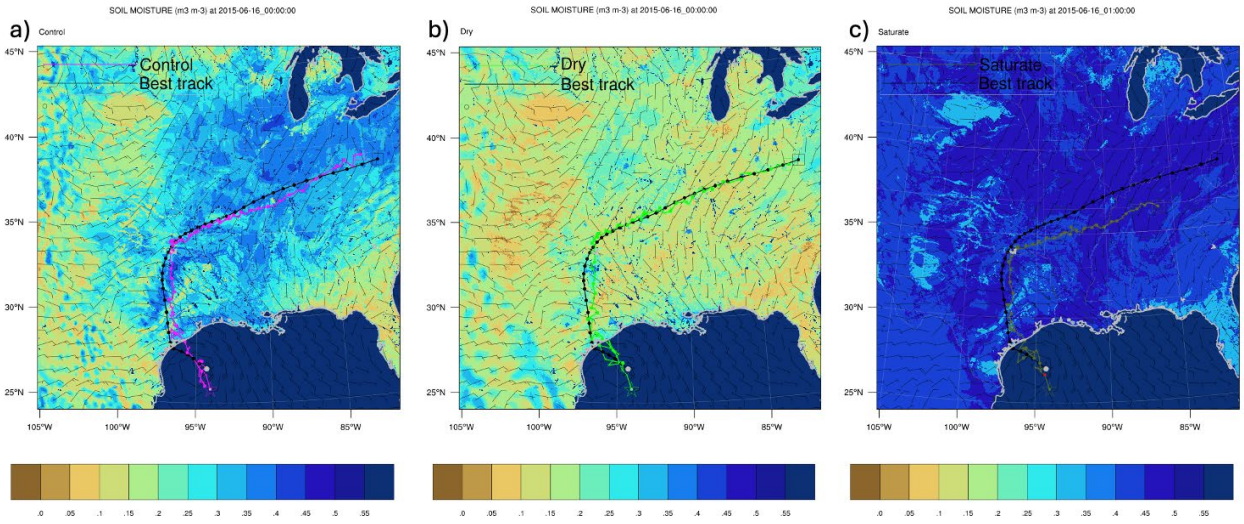

Figure 2. Initial soil moisture conditions of a) Control, b) Dry, and c) Saturate cases in the NU-WRF main simulations.

In terms of experimental design, LIS and NU-WRF are configured with a 1 km grid spacing over a 2400 by 2400 grid domain in Lambert coordinates along with 60 vertical layers (Fig. 2). The domain covers more than the entire central U.S. geographically where Tropical Storm Bill traversed for its entire lifecycle from its genesis to lysis. The domain was designed to fully capture these TCMIs considering the size of the storm's environment as well. We applied the same NU-WRF physics suit with Goddard 4ICE microphysics option, Goddard 2017 radiation schemes, MYNN2 PBL and surface layer option for all the simulations identically except the YSU PBL scheme permutation.

2.2. Backward Trajectory Analysis (BTA)

The general spiral structure of TC or hurricane cloud is well known (e.g., Franks 1977; Anthes 1982) during their development and mature stages. After the landfall of TCs even in tropical latitudes, most TCs weaken rapidly even without interacting with any dry air masses (Anthes 1982). It was considered that the large reduction in LHF would occur as TCs leave the ocean, immediately shutting off the significant portion of water vapor for convection, thus, rapidly diminishing condensation and latent heating within the core of the storm needless to say the relatively cooler land surface with the increased surface roughness compared to the warm and

relatively flat ocean surface (Anthes 1982). Due to these general behaviors of TCs after landfall, the dynamic structure of TCs after landfall has not been vigorously investigated compared to those of the other phases of the TC life cycles. However, as noted in the introduction, more than a few TCs that went through reintensification processes after landfall posed major threats to the inland communities, necessitating a better understanding of the dynamics of landfalling TCs that go through the TCMIs.

To better understand the TC inflow dynamics and wet soil impacts on the TCMIs, we implemented the NOAA HYSPLIT model (Draxler and Hess 1998; Stein et al. 2015) to calculate the temporal evolution of multiple aspects of the air parcels (e.g., specific humidity, temperature, elevation, etc.) that converged into the core of the Bill at both 500 m and 3000 m heights after landfall of the storm. HYSPLIT is a comprehensive system that can be used for simple air parcel trajectory calculations, as well as more complex simulations of transport, dispersion, chemical reactions, and deposition. HYSPLIT is widely used in the atmospheric sciences community over more than 30 years and has over 800 citations on Web of Science (Stein et al. 2015). One of the most common model applications is a back-trajectory analysis to determine the origin of air masses and establish source–receptor relationships (Fleming et al. (2012) and references therein). Also, the HYSPLIT model has been widely used in a variety of studies in combination with the WRF model. For example, it has been used to study landfalling tropical cyclones (e.g., Wakefield et al. 2021), extratropical cyclones of type Vb that develop in the Western Mediterranean and head into Central Europe (Messmer et al. 2020), and air quality forecasting (Yerramilli et al. 2012). In a Lagrangian framework, back trajectory analysis of air parcel helps us comprehend the evaporative sources of water vapor for the TCMIs. In particular, since moisture flux from the land surface reaches mid-to-upper-level atmospheres through the PBL, the diurnal cycle dynamics of the PBL (Sodemann et al. 2008) play an important role during TCMIs. Application of HYSPLIT to the coupled NU-WRF simulations can therefore help enhance our understandings of the moisture energy budget between land surface and lower troposphere during the TCMIs.

For the HYSPLIT analysis of TS Bill, we used hourly outputs of the NU-WRF model simulation for 48-hour BTAs. Spatial distribution of the trajectory seed location consists of 25 azimuth angle legs on ten radial rings at 0.1, 0.2, 0.5, 0.7, 1, 2, 3, 4, 5, and 6 arc degree distances

from the moving center of the storm (total of 250 seed points) (Figure A3). Inner radii are defined at 0.1 ~ 0.7 arc degrees (approx. radius < 80 km) while outer radii are defined in between 1 and 6 arc degrees from the center of the simulated storm in motion (approx. 100 km < radius < 660 km). Those trajectory seeds are released every six hours (i.e., at 00, 06, 12, and 18 UTC) at the heights of 500 m and 3000 m AGL along the TC tracks.

3. Model Validation and Observational Datasets

Both quantitative and qualitative model validations have been sought for the Control run using radiosonde observations from the U.S. Department of Energy (DOE) Atmospheric Radiation Measurement (ARM) Southern Great Plain (SGP) site, Oklahoma mesonet data, and NOAA NEXRAD radar images as well as the Best Track dataset. The Enhanced Soundings for Local Coupling Studies Field Campaign (ESLCS; Ferguson et al. 2016) took place at the ARM-SGP Central Facility (CF) from 15 June to 31 August, 2015. The ESLCS was conducted to sample the evolution of the daytime planetary boundary layer (PBL) using high temporal (~hourly) resolution radiosondes (1) to improve understanding and modeling of the diurnal evolution of the PBL, particularly with regard to the role of local soil wetness, and (2) to bring new insights into the appropriateness of ARM-SGP CF thermodynamic sampling strategies. During the field campaign, the passing of TS Bill occurred near the site on 18 June and this day was specifically chosen as a unique opportunity for intensive observing period (IOP) to capture PBL evolution during TC passage. We compare our NU-WRF simulation results to the ESLCS observational records during its IOP period on June 18, 2015. Figure 3 suggests that temperature profile (red line) was closely reproduced in our Control run (red dashed) from the surface to upper-level atmosphere. Also, atmospheric moisture profile was reproduced relatively well, in particular, in the lower-level troposphere up to 700 hPa, although the Control case did not reproduce the dry mid-level atmosphere in the ARM SGP radiosonde, which is attributable to dry air intrusion from the north to the west of TC core. The vertical wind profile wind barbs in Fig 3 also suggest that the measured and simulated wind directions did not match each other especially in the lower-to-middle atmosphere. The dry mid-level atmosphere over the ARM SGP could have been missed by the model potentially due to several reasons: time difference between the actual radiosonde observations along with its own drift and our simulation outputs for the straight vertical profile and/or the model's track error. However, nevertheless, our thorough (and

various) analysis results suggest that our simulations and overall performance were not critically affected by the local feature of the dry mid-level atmosphere missed over a specific location within the large domain.

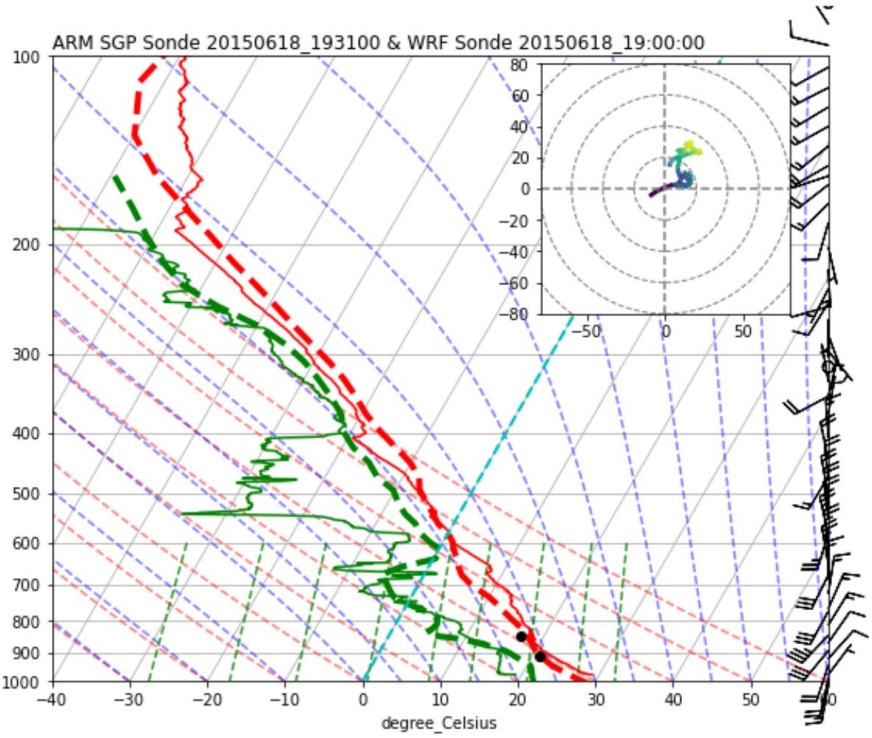

Figure 3. SkewT plot comparing the radiosonde from ARM SGP at 19:31 UTC (lines) and the vertical profile from Control run (dash lines) at 19 UTC on 18 June, 2015.

Comparison between Oklahoma Mesonet dataset and the Control run suggested that LIS spinup was able to reproduce the horizontal distributions of soil moisture and temperature at the top level soil layer (5 cm) very close to the observation data throughout state (not shown). Qualitative comparison of composite radar reflectivity animation of the Control run with the NOAA NCEI NEXRAD as well as GOES Infrared satellite imagery (available at https://vortex.plymouth.edu/tropical/archived_data/2015/atl_2015_sum.html#bill) suggests that the Control run reproduced the spiral structure of TS Bill and cloud distribution around the storm very well from the time of landfall and throughout the TCMI period (Figure A4). Control run (i.e., gdas case) reproduced the radar reflectivities of the NEXRAD imagery better than the NLDAS2 case.

4. Results

4.1. TS Bill Evolution over Land

Simulated tracks were quite comparable among all the permutation cases with the observed record as shown in Fig. 1e and Fig. 4. Note that Saturate and NoahMP cases produced slow storm speed compared to the others, making their track shorter than the others. Considering that TCs often move slower over a warm sea surface area (e.g., over a warm Loop Current in the Gulf of Mexico), their slow translations of the storm seem to be related to the higher soil moisture with higher surface enthalpy condition than the other cases. In contrast, there were large differences in storm intensity among permutation cases during the TCMI period of interest on 19 June as shown in Fig. 5. Compared to the Best Track intensity record, each of the simulations took ~48 hours to fully reach their equilibrium of the TC's dynamic state in 1 km grid resolution within in the 2400 km by 2400 km single domain. These first 2 days can be considered the TC spinup period, after which the simulation were able to reproduce the observed storm intensity from 18 June on and show a spread of storm intensity during the TCMI period. In particular, Control and NLDAS2 cases reproduced the TCMI of the storm very close to the observations, with a clear deepening of the storm (decrease in pressure) simulated during the TCMI period. In addition, YSU and NoahMP maintained their intensity during the TCMI period. In contrast, Saturate, Dry, and NoLHF cases failed to reproduce any TCMI, and show a consistent inland weakening and rising pressure throughout the period. Combined with the analysis in Fig. 1 regarding simulated vs. observed (Best Track), results lend confidence that the NU-WRF simulations represent the track, timing, and inland intensification reasonably well such that the permutations in Tables 1 and 2 produce physically meaningful and realistic results regarding the actual and potential behavior of TCMI in TS Bill under varied surface conditions.

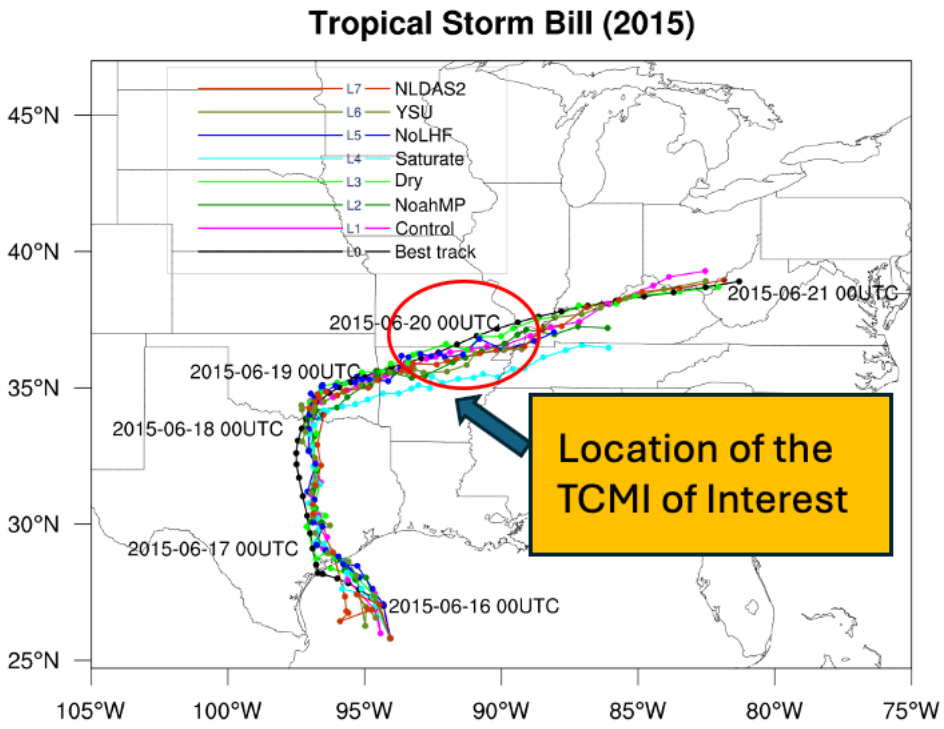

353

354 Figure 4. Simulated storm's tracks of NU-WRF main simulation permutations along with the
355 best track record.

356

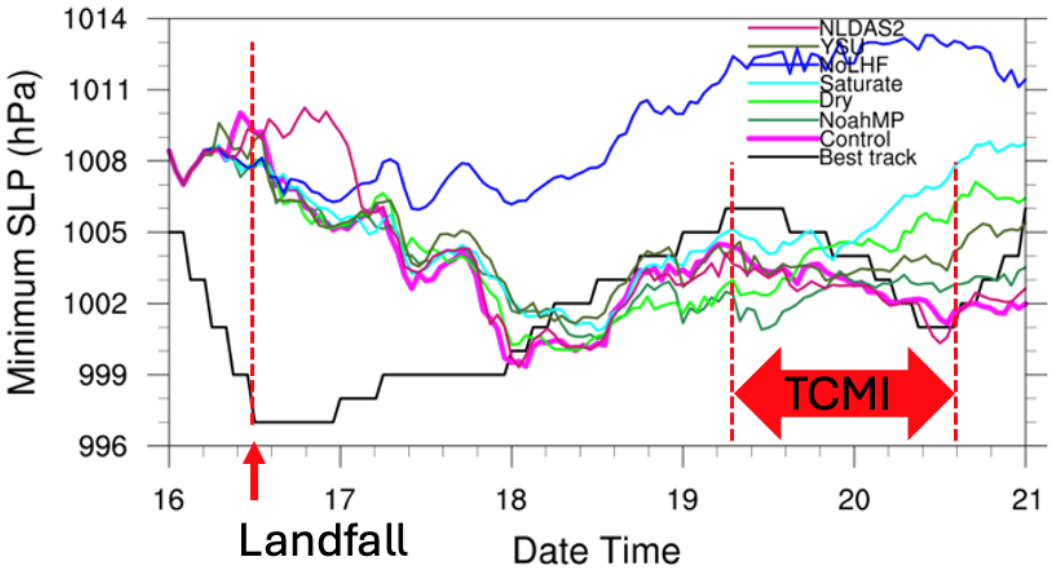

357

358 Figure 5. Time series of simulated storm intensity in minimum sea level pressure (hPa) along
359 with the observed storm intensity. Approximate times of landfall and TCMI of the storm are
360 noted with dashed lines.

4.2. Land Surface Energy Balance Perspective

Given the focus of these permutations on understanding the role of surface/soil moisture on TCMI, it is important to consider the impact of soil moisture on surface turbulent fluxes, the latter being what is ultimately communicated from the land (LIS) to the atmosphere (NU-WRF) (i.e. the process-chain described in Santanello et al. 2018). To properly understand the water and energy budgets of the simulated storm, time series of the spatial integral of Latent Heat (LHF) and Sensible Heat Flux (SHF) within a 100 km radius and 600 km radius were calculated. Total LHFs within 100 km radius (Fig. 6a) were quite comparable among all the cases (except the NoLHF case, as prescribed), which was attributable to the widespread cloud cover in the inner core of the simulated storm. With the limited incoming solar radiation in the TC core area, Dry case produced more LHF than other cases with wetter soil moisture. The negative SHFs within the 100 km radius suggests that the incoming solar radiation was near zero in the TC core area where it was precipitating (Fig. 7a). These results reverse for the 600 km radius where incoming solar radiation was more abundant in the outer core area with limited clouds (Fig. 7b). The Dry case produced less than 2/3 of LHF of the other wetter soil moisture cases during the peak of the diurnal cycle. Also, it is notable that the Saturate case produced less LHF than the other cases with wetter soil, which can be associated with the further expanded clouds in the TC core as well as the cooling effect of the saturated soil shown in Fig. 7b. Overall, the clear diurnal cycles in the surface enthalpy fluxes of landfalling TCs suggest that the landfalling TC are highly dependent on and subject to the diurnal cycles of solar radiation which regulate the surface enthalpy fluxes over the land. At the same time, initial soil moisture has larger impacts on surface enthalpy fluxes in the outer core region without thick clouds than inner core region under heavy clouds. The difference in LHF between Control and NoLHF can also be thought of “the net Brown Ocean Effect” of soil moisture on the TCMI of TS Bill.

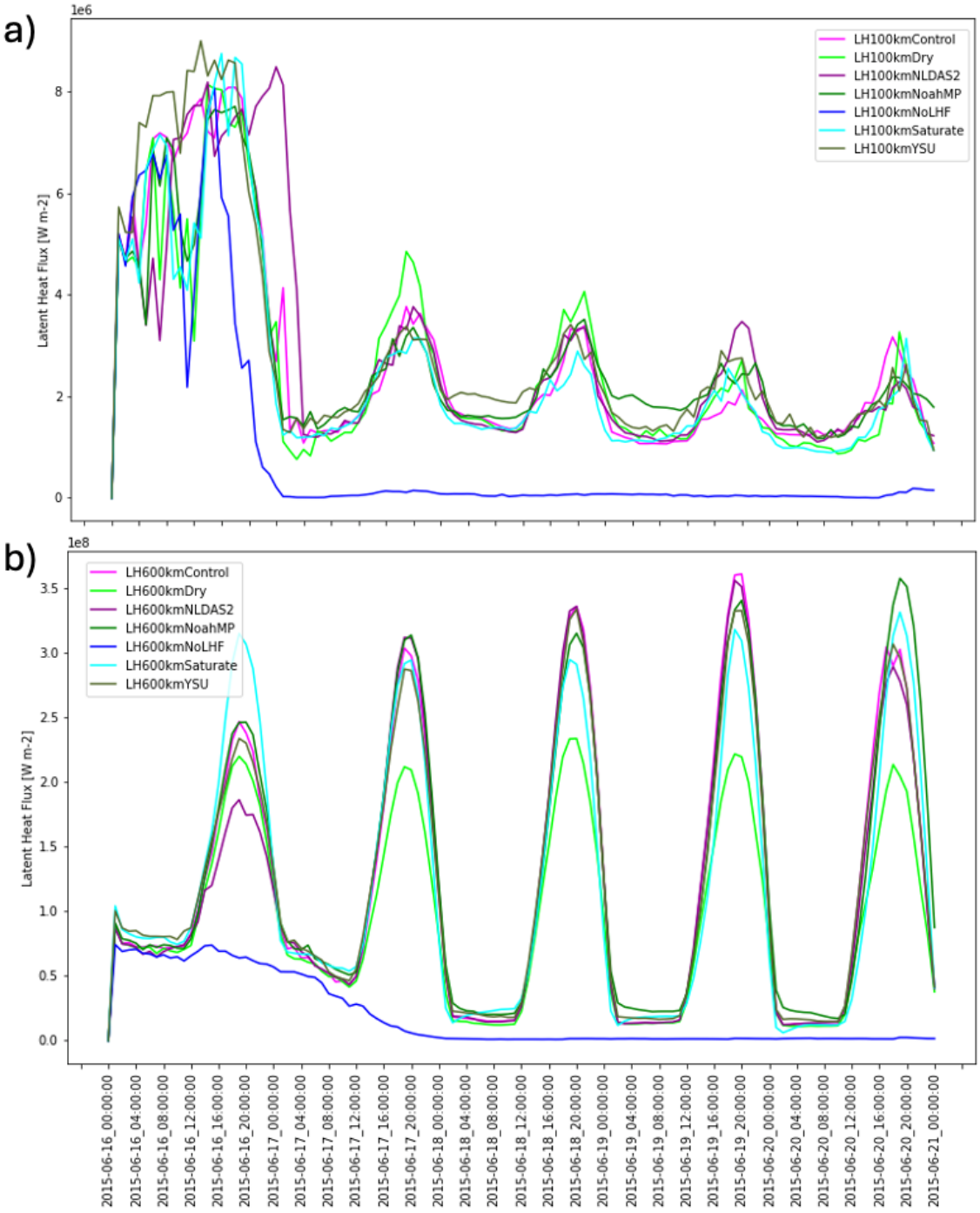

388

389 Figure 6. Time series of the spatial integral of LHF within the circular areas of 100 km
390 (a) and 600 km (b) radius from the center of storm of all the permutation cases.

391

392

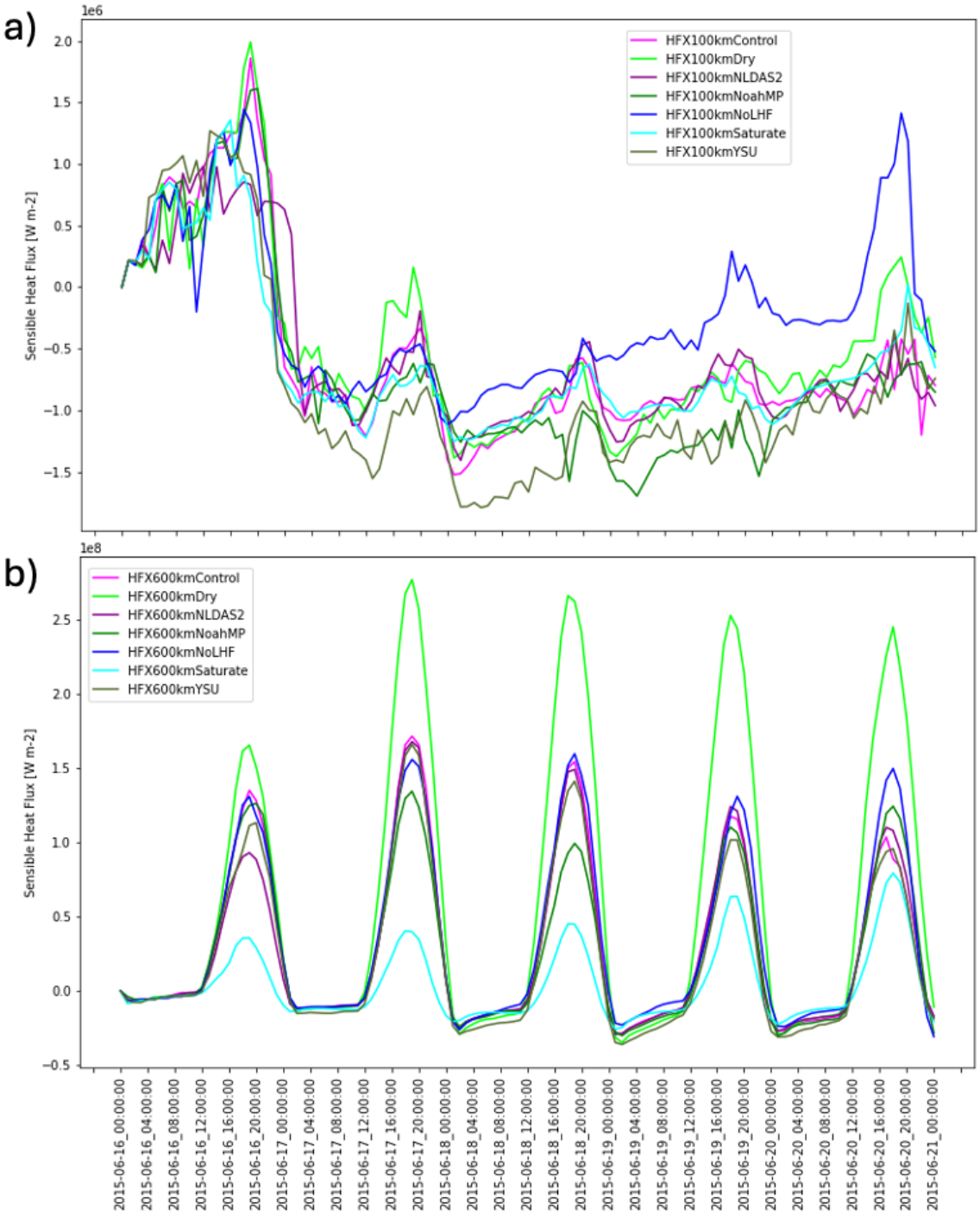

393

394 Figure 7. As in Fig. 6 but for sensible heat flux.

395

Likewise, time series of the spatial integral of Total Precipitable Water (TPW) within 100 km radius and 600 km radius were calculated (Figure 8). In general, the landfalling TC core is embedded within the moisture advection from the ocean. While the TPW amounts decreased gradually as the center of the storm moved into the inland, the TPW in the vicinity of TC core is the product of the advected airmass that interacts with the land surface in the path. Fig. 8a shows that TPW experienced substantial increases before and during the TCMI period in all the cases except NoLHF case which had a monotonically decreasing TPW trend over land, resulting in no TCMI. Control and NLDAS2 cases had the largest gain in the TPW among the permutations during the TCMI period followed by YSU, NoahMP, Dry, and Saturate. This suggests that the diurnal cycle of LHF from the land surface is closely correlated with the TPW in terms of its impact on the water vapor amount in the lower atmosphere. Notably, the magnitudes of mean TPW increase were higher in the inner core area (about 5 [kg m-2]) than in the outer-core region (about 2 [kg m-2]), while the LHFs in the outer-core region were roughly more than ten times larger than those in the inner-core area (Fig. 8b). This discrepancy is likely due to 1) more water vapor is being funneled into the inner-core area than outer-core region from off-shore due to the pressure gradient perpendicular to the inflow stream and 2) surface moisture flux (e.g., LHF) from outer-core region advected (was pulled) into the inner-core area during the TCMI period effectively. Figure 9 supports that the TCMI process of TS Bill over the Central U.S. produced extreme amounts of precipitation on June 19 compared to average monthly precipitation climatology in June (base period of 1991-2020) from the NOAA Monthly U.S. Climate Gridded Dataset (NClimGrid; Vose et al. 2014). The TCMI area (shown in red circle in Fig. 9a) gets below 4 inches of rain in June climatologically, which is consistent with below 2.6 or 2.2 inches of precipitable water climatology measured by rawinsonde data (Schroeder et al. 2016) at Springfield, MO (period of record 1998-2022) and Little Rock, AR (period of record 1995-2022) during June, respectively (not shown; see https://www.spc.noaa.gov/exper/soundingclimov2/). However, NOAA National Centers for Environmental Information (NCEI) Cooperative Observer Program (COOP) Hourly Precipitation Data (HPD) version 2 (Wuertz et al. 2018) shows that daily maximum precipitation observed in the vicinity of Bill's TCMI location (red circle in Fig. 9 b) reached up to .75~1.80 inches during the TCMI on June 19 (Fig. 9c). More in-depth analysis for this aspect of moisture advection will be explored in terms of the 3-D nature of TC advection and fuel in the following section.

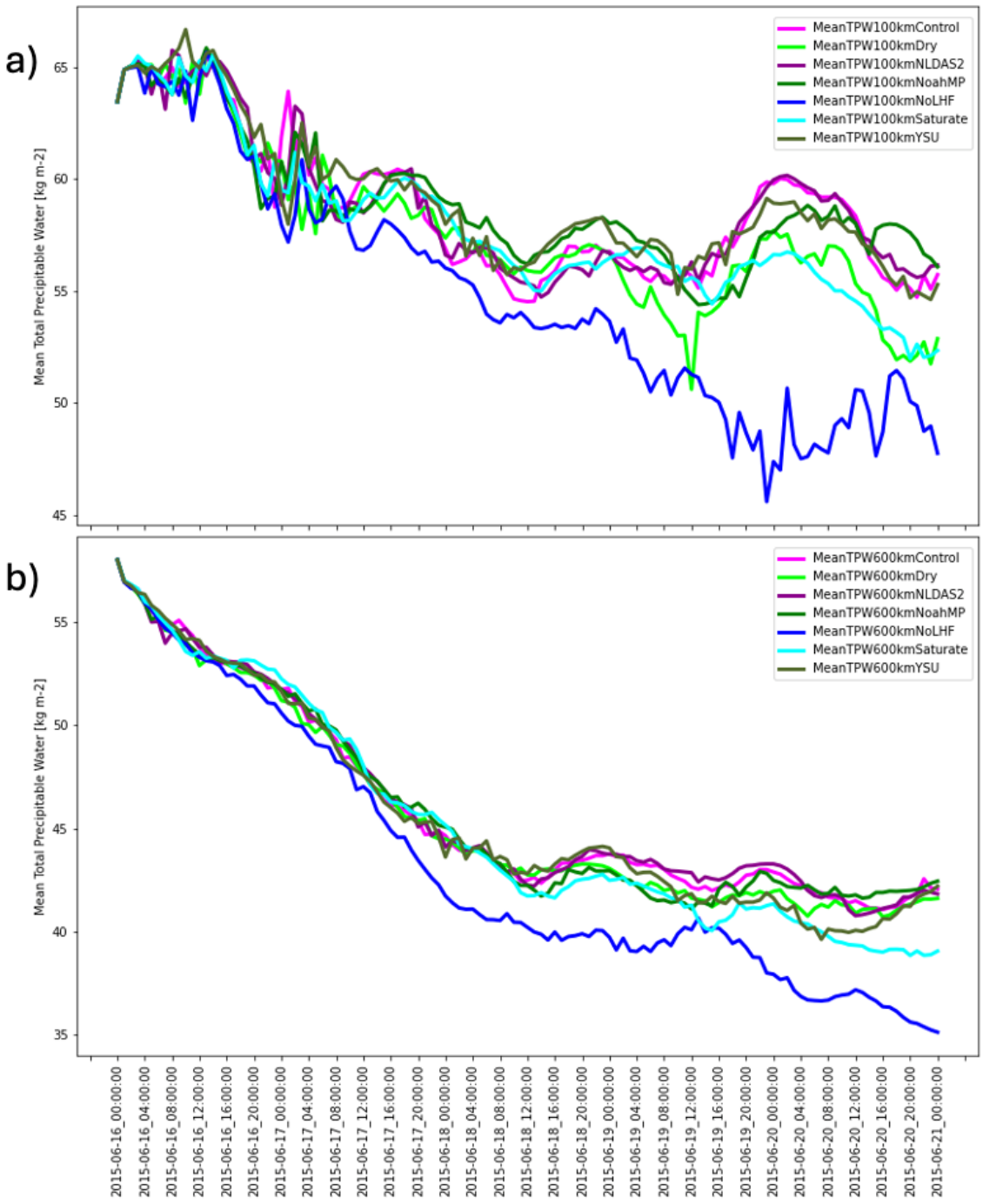

Figure 8. As in Fig. 6 but for Total Precipitable Water (TPW).

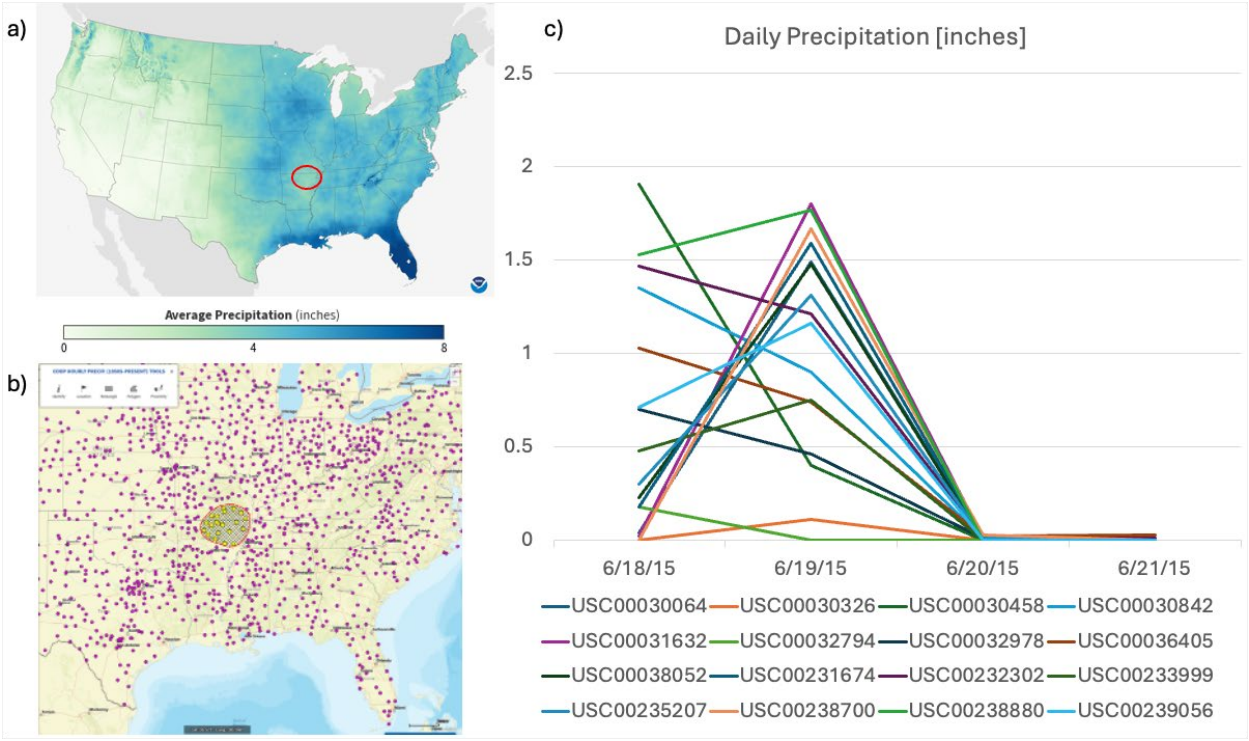

Figure 9. a) Average monthly precipitation climatology in June (base period of 1991-2020) from the NOAA Monthly U.S. Climate Gridded Dataset (NClimGrid), b) NOAA National Centers for Environmental Information (NCEI) Cooperative Observer Program (COOP) Hourly Precipitation Data stations selected in the vicinity of Bill's TCMI location (red circle), and c) daily precipitation records during the passage of TS Bill (June 18~21, 2015) over the Central U.S. measured by the selected stations in b).

4.3. HYSPLIT 48-hour backward trajectory analysis

a) Dichotomy of inflow air mass dynamics in the TC: Differences in air mass properties by distances from center of storm and altitude

As described in the BTA section, we strived to investigate the complex dynamics of landfalling TCs by focusing on the storm's convergence flows at 500 m AGL and 3000 m AGL. 500 m is considered as the mixed layer height within TC core over the ocean in general (Gopalakrishnan et al. 2016; Montgomery et al. 2006) and the 3000 m is the approximately maximum altitude of Lifting Condensation Level (LCL) even under the TC environment. Figure 10 a and c suggest that the TC PBL (~500 m above ground level (AGL)) was interacting with and dominated by the airmass that was advected from the Gulf of Mexico (GOM) in the south of the storm almost exclusively, even up to 600 km radius from the center inland in the Central U.S. In contrast, the TC inflows at the 3000 m level (Fig. 10 b and d) were experiencing the dry air intrusions both from the mid-latitude and tropical latitudes. These distinct inflow patterns at 500 m and 3000 m AGL clearly sustained from the early stage of landfall and throughout the TCMI process of TS Bill. In particular, the dominant inflows from the GOM into the TC PBL lasted much longer than previously conjectured by the general TC research community, about one day.

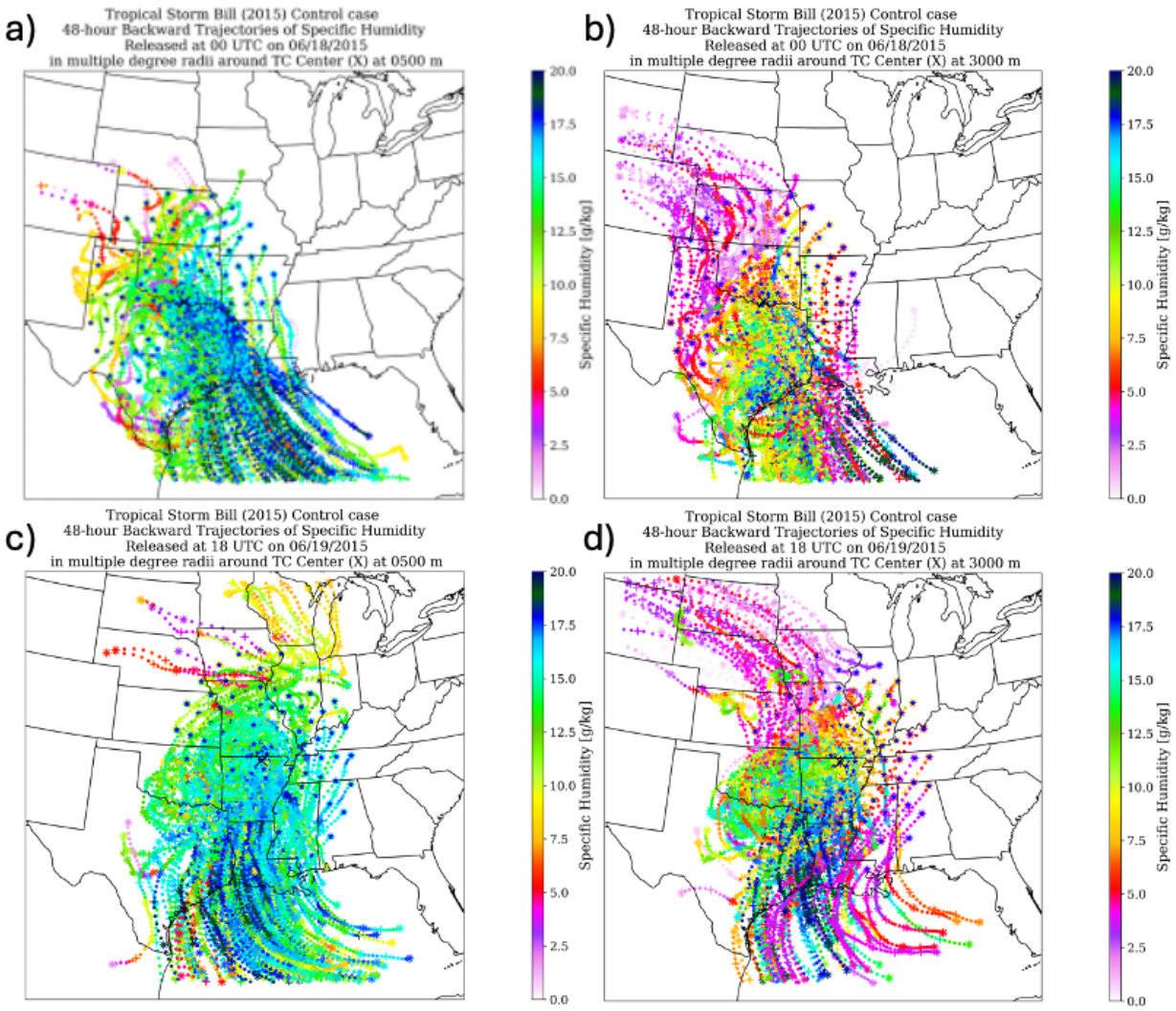

458

459 Figure 10. 48-hour back-trajectory analysis of air parcel's specific humidity of TS Bill in the
460 Control case with the trajectory seeds (annotated with blue stars) released at a) 500 m and b)
461 3000 m AGL at 00 UTC on 18 June when the storm center (annotated with "x") was about to
462 cross the Texas-Oklahoma boarder approx. one day after its landfall and c) 500 m and d) 3000 m
463 AGL at 18 UTC on 19 June when the storm went through TCMI process approx. three days after
464 its landfall.

465 This dichotomy of inflow airmass in the landfalling TC can be better understood by
466 separating the back-trajectories into two groups, the inner-core and the outer-core of the storm.
467 In this study, the inner-core of TC is defined as the TC core area within a radius of 100 km from
468 the center of the storm. The region beyond the 100 km radius is considered the outer-core of the
469 storm. It becomes clear that this separation of the inflow regions into two regions is highly
470 effective in differentiating their characteristic airflow patterns within the TC environment as

shown in Fig. 11. In the TC PBL (Fig. 11 a and b), the inflows to the inner-core of the storm are funneled almost directly from the GOM with very high specific humidity levels (>18 g/kg) retained even over land. In contrast, the inflows into the outer-core are of lower specific humidity (<16 g/kg) and they had more circuitous routes of flow when their trajectory seed origins were over land (not shown). Temporal evolution of air parcel's features (i.e., altitude, moisture flux, PBL height, and specific humidity in Fig. 11) suggests that air parcels into the inner-core of the storm passed through the lower altitudes (i.e., AGL) within the PBL more than those into the outer-core region. Temporal moisture flux plots also suggest that the air parcels in the inner-core "funnel" did uptake the more moisture from the surface than the counterparts. Within the inner-core funnel, the PBL heights (PBLHs) that the individual parcels traveled within stayed relatively low (~ 1 km) during the 24 hours of trajectory while those to the outer-core region passed through a more dynamic PBL that fluctuated with the diurnal cycle. Temporal evolution of the specific humidity also suggests that the air parcels in the inner-core funnel gained moisture gradually through the inflow and their final specific humidity converged within the range of 12 to 18 g/kg. In contrast, those for the outer-core region did not vary much through the trajectories with quite a good portion of drier air as well as the larger spread of the specific humidity (8 ~ 18 g/kg) at their final stops at 00 UTC 18 June. Similar patterns of these differences between the inner-core and outer-core inflow trajectories can be found with the 3000 m seeding levels as well (not shown), where the more mid-latitude dry air masses were transported into the TC outer-environment. As a result, the inner-core of the landfalling TC tends to pull in more moist air than the outer-core.

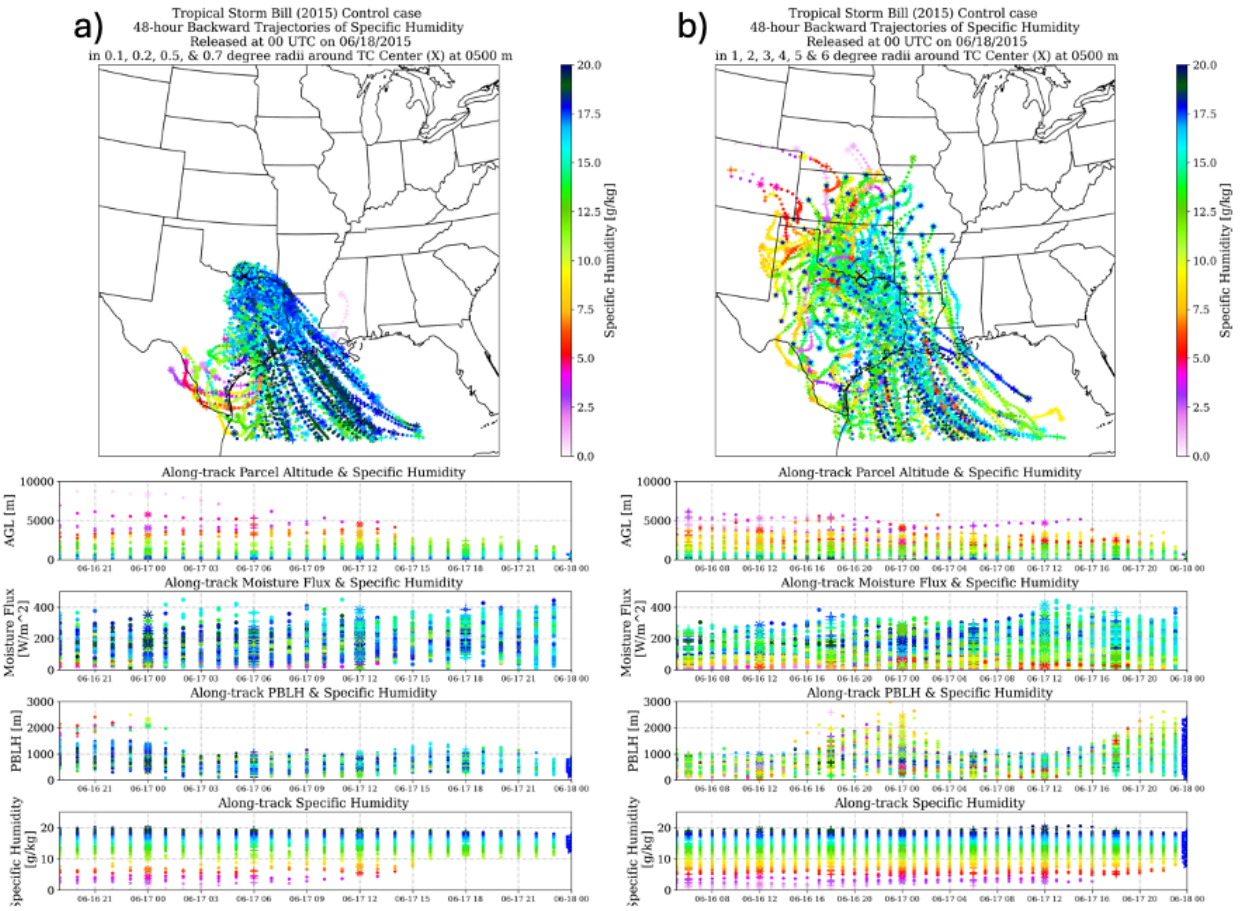

Figure 11. 48-hour back-trajectory analysis of air parcel along with temporal evolutions of parcel features for the Control case. Trajectory seeds were released in a) the inner-core (< 100 km) and b) the outer-core (<600 km) at 500 m AGL at 00 UTC on 18 June approx. one day after landfall.

b) Soil moisture and LHF interaction with inflow streams

The same 48-hour backward trajectory analysis was applied to Dry, NoLHF, and Saturate cases to quantify the sensitivities of the inflow air parcels to the surface moisture conditions up to the onset of the TCMI of TS Bill. Figure 12 shows that air parcels into the inner-core area tend to start with higher specific humidity levels than those into the outer-core region as they originate from the GOM regardless of the soil moisture permutations, which is associated with the spatial wind speed distribution over the ocean as the higher wind speeds can produce the more LHF from the ocean surface. In Control case (Fig. 12a), these high specific humidity levels are well maintained up to the inner-core of the storm far inland. In contrast, parcels in Dry case (Fig. 12b) lost moisture during the passing over dry land in the Texas-Louisiana border and

Arkansas (see Fig. 2b). Likewise, almost every air parcel in NoLHF case started to lose their moisture as soon as they crossed the coastline since they were not supported by any LHF from the land surface. This NoLHF case suggests that a moist low-level jet advected from the ocean can dissipate rapidly over the dry land. Saturate case (Fig. 12d) seems to be able to maintain the moist low-level jet up to the inner-core area due to the saturated soil. In particular, when single trajectories were inspected (not shown), it was found that air parcel's specific humidity had increased after passing over long patches of wet soils in Control and Saturate cases (see Fig. 2 a and c). These moistening trajectories are easily noticed in the outer-core plots of Control and Saturate cases (Fig. 12 e and h), which seldom occur in Dry and NoLHF cases (Fig. 12 f and g).

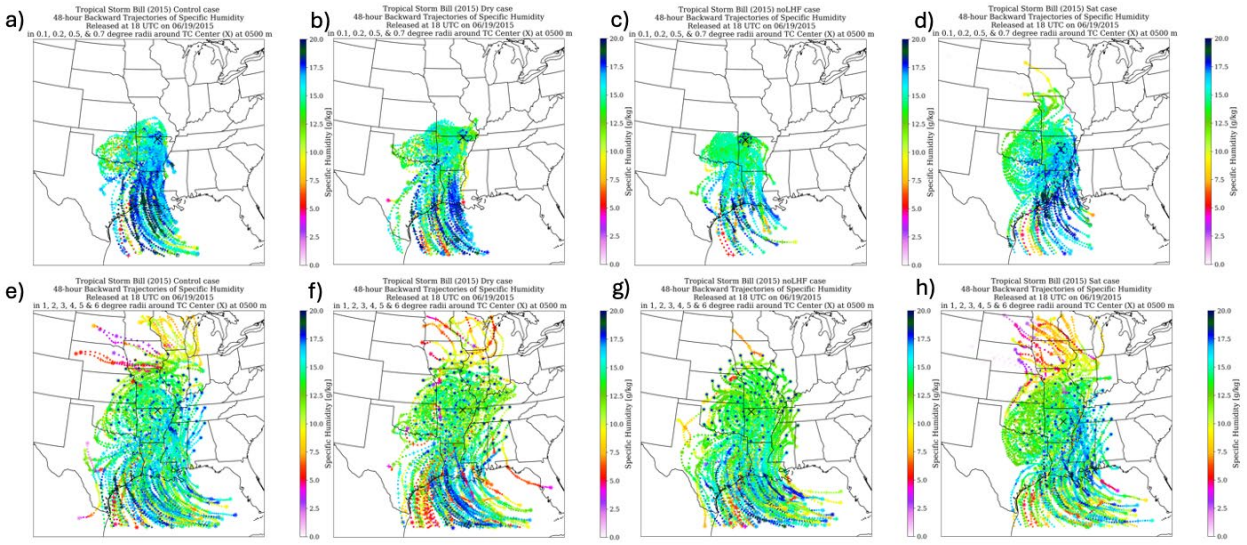

Figure 12. 48-hour back-trajectory analysis of Control (a and e), Dry (b and f), and NoLHF (c and g), and Saturate (d and h) cases for the inner-core (top) and the outer-core (bottom) regions with seedings released from 500 m AGL at 18 UTC on 19 June. Red-green-blue color scale of trajectories represents specific humidity level of the air parcels.

4.4. Three-dimensional visualization of soil moisture impacts

Using the NCAR VAPOR visualization software, the three-dimensional evolutions of the atmospheric moisture distributions were investigated during the onset of TCMI of TS Bill at 18 UTC on 19 June 2015. Because L-A interactions were of our key interest, the evolution of the low-level atmospheric moisture distributions was co-plotted with the evolution of the surface LHF for the Control, Dry, NoLHF, and Saturate simulation cases (Fig.13). Considering that TC development requires at least 12 g/kg of water vapor in the lower atmosphere empirically, air mass with more than 16 g/kg of water vapor can be ample to support an existing TC in terms of

enthalpy supply. Figure 13a suggests that the moist land surface in Control was able to supply the required enthalpy to the core of the storm far inland from most of the azimuth directions to the center through the strong surface moisture flux over the Central U.S. and the advection from the GOM. In contrast, the very weak surface moisture flux from the land surface in Dry case failed to sustain the ample moisture supply in most of the azimuth directions to the storm's center except the area in the southwest where the soil was precipitated by the storm itself during landfall (Fig.13b).

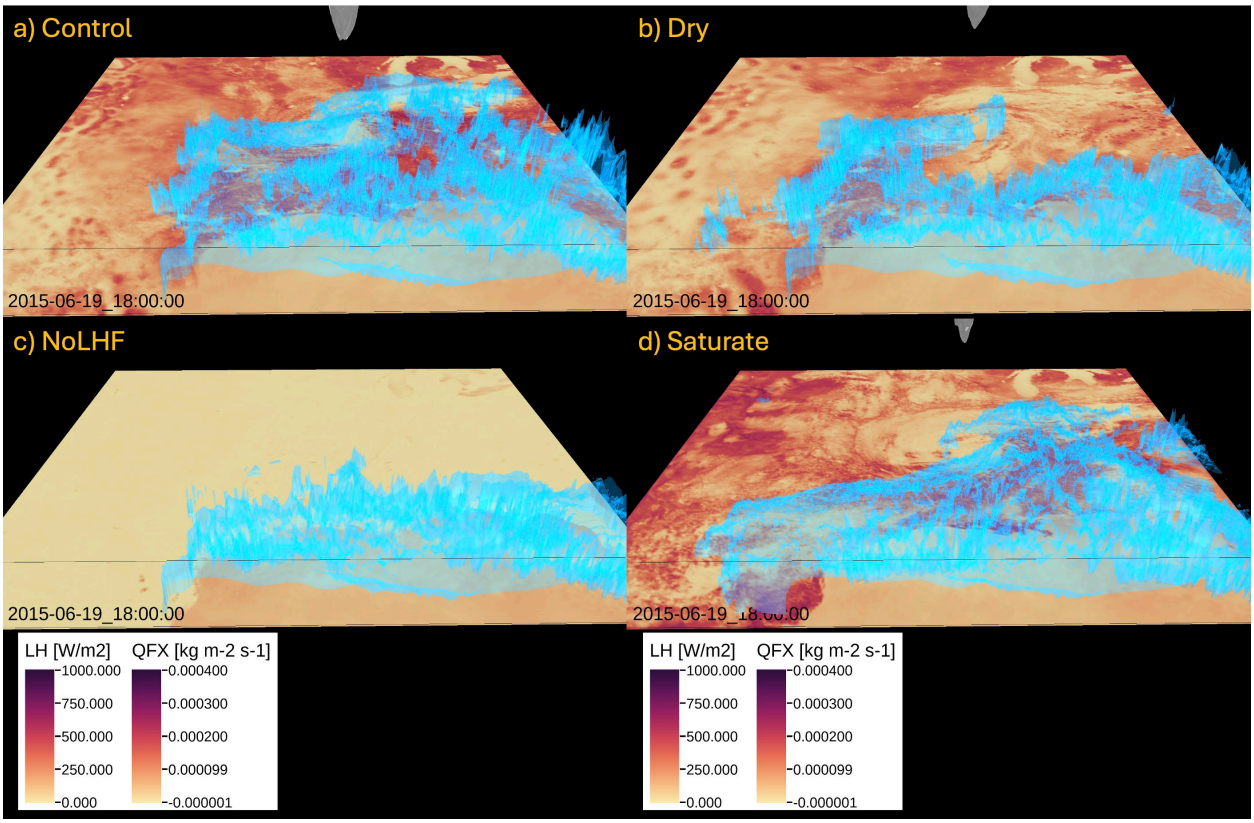

Figure 13. Comparison of the atmospheric moisture distributions during the onset of TCMI of TS Bill at 18 UTC on 19 June 2015 among a) Control, b) Dry, c) NoLHF, and d) Saturate simulation. Iso-surfaces of the QVAPOR at 16 g/kg are visualized in blue which is superimposed over the surface moisture fluxes in LH (latent heat) and QFX (surface moisture flux). The gray tip at the top center of each panel is part of 3D renderings of perturbation pressure at 120 Pa from the base state pressure in 3D, which indicates the center of the simulated storm underneath it.

NoLHF case suggests that the strong evaporation continued over the GOM during the TCMI of the TS Bill (Fig.13c). However, the land surface without LHF diminished the atmospheric moisture substantially below the 16 g/kg over the land, which prevented the TC

from sustaining or intensifying over the land. With the fully saturated soil, Saturate case (Fig.13d) had a large basin of the high atmospheric moisture (> 16 g/kg) in the south and in the east of the storm, which was similar to Control case. However, latent heat fluxes in the west of the storm were much weaker than those in the Control case, which seems to be associated with the active cloud formation in that direction as well as the extended TC cloud about the center due to the saturated soil.

4.5. Land-Air coupling during the TCMI event

The role of the PBL and L-A coupling in the TCMI is another key area of interest in the study. For this purpose, we applied the Local L-A Coupling (LoCo; Santanello et al. 2009, 2011a, b) metrics to our NU-WRF main simulation permutation cases (Fig.14). The LoCo metrics were composed for the storm center location at the time of TCMI by the Best Track record valid one day prior (18 June) to the TCMI itself in order to examine the state of L-A coupling that exists in the TCMI region across these permutations. It is evident that DRY run stands out as an outlier in terms of all the aspects of heat and moisture energy evolution, PBL growth and entrainment, and surface fluxes (i.e., Evaporative Fraction). These L-A feedbacks 'precondition' the DRY run towards a less favorable condition for the TCMI, where the LCL deficit also became large in the local afternoon in the DRY run, indicating a tendency away from the LCL being reached due to drier surface conditions.

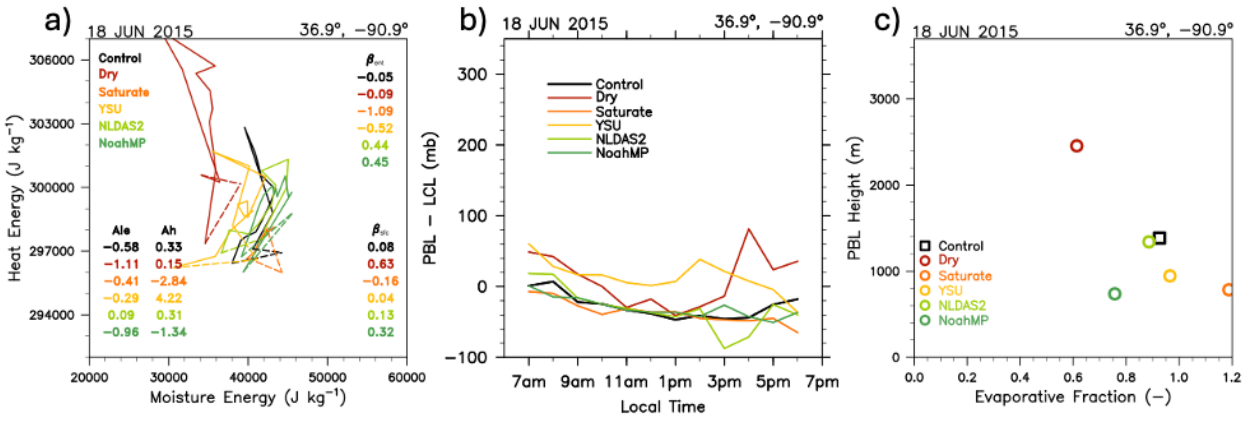

Figure 14. LoCo metrics of a) mixing diagrams of heat and moisture energy space and PBL growth and entrainment, b) LCL deficit, and c) Evaporative Fraction vs. PBL height (Santanello et al. 2009, 2011a,b) for Control, Dry, Saturate, YSU, NLDAS2, and NoahMP permutations.

5. Summary and Discussion

In this study, the impacts of soil moisture, surface energy balance, and L-A interactions within the TC inflow environment that preceded and supported the TCMI of TS Bill were assessed using the NASA NU-WRF modeling framework as well as NOAA HYSPLIT back-trajectory analysis. NASA's LIS and NU-WRF were executed in three phases: LIS Spinup, Pilot Runs, and Main Simulations. Through the LIS spinup within the NU-WRF, we reconstructed realistic soil moisture conditions during TS Bill and simulated TS Bill's inland lifecycle which compared well with observed storm track and intensity trends. After selecting the best performing Control case, quantitative and qualitative model validations were conducted using various observation datasets such as OK Mesonet weather network, ARM-SGP radiosondes, NEXRAD radar imagery, satellite imagery, as well as the best track data.

The Main Simulation phase involved thorough analyses of NU-WRF permutations using energy budget analysis, HYSPLIT back-trajectory analysis, 3-D visualization, and land-atmosphere (L-A) coupling metrics. Our findings revealed dynamic interactions between land surface enthalpy conditions (latent and sensible heat fluxes) under the TC inflow channels and the inflowing air parcels across the inner core, outer core, and TC background environment. Notably, comparisons of back-trajectory analyses between Control, Dry, and NoLHF cases effectively demonstrated how wet (dry) soil moisture can support (inhibit) the TCMI of a landfalling storm far inland through dynamic L-A interactions. These interactions involve the exchange of moisture and energy between the wet (dry) land surface and inflowing air streams within the boundary layer, ultimately impacting the storm's core. Furthermore, we found that moisture advection from the ocean to the inland TC core was significantly influenced by active L-A interactions within the boundary layer. In this layer, inflowing air's water vapor pressure rapidly equilibrates with that of the underlying soil surface, whether moist, dry, or saturated. The degree of this moist/dry equilibrium depends on the length of the advection fetch. During moist assimilations, air parcels could become even more moist over land than over the ocean, enabling TCMI or the Brown Ocean Effect. Our comprehensive investigation of the spatial and temporal dynamics strongly suggests that Tropical Storm Bill exemplifies a clear case of TCMI fueled by a substantial supply of latent heat flux from the land (via soil moisture preconditioning), thereby supporting the concept of the Brown Ocean Effect.

This study provides compelling evidence for the unique mechanisms that precondition and support Tropical Cyclone Maintenance and Intensification (TCMI) during Tropical Storm Bill's landfall and inland evolution. Our findings highlight the complex interplay between the land, ocean, and atmosphere across multiple scales, challenging traditional understandings of tropical cyclone behavior after landfall. Recognizing this complexity is crucial for accurately assessing and predicting the likelihood of TCMIs ahead of a landfall, ultimately safeguarding human lives and property. By meticulously examining cases like Tropical Storm Bill and Tropical Storm Kelvin (Yoo et al., 2020), we can gain a more comprehensive understanding of the Brown Ocean Effect. This study, along with previous research, conclusively demonstrates that the Brown Ocean Effect is not a binary phenomenon but operates on a continuum, exerting a varying degree of influence on the tropical cyclone as it moves inland.

6. Implications for Future TCMI Likelihood and Prediction

Through the study of the TS Bill, authors speculate on three major factors that control TCMI event: moisture availability, incoming solar radiation on the land, and vapor pressure temperature in the boundary layer. Moisture can be available either by low-level jet from the ocean (i.e., advection) or wet soil, which is a fundamental element of the TCMI. Secondly, the amount of incoming solar radiation becomes critical especially with high soil moisture, where cloud fraction plays a key role in the yield of LHF. Finally, temperature in the lower PBL or at the surface determines the vapor pressure deficit of the air mass above the surface, which in turn can dictate both the amount of moisture that can be incorporated by the air parcel as well as the LHF from the soil surface. Figure 15 shows the scatter plots of air temperature (T_{air}; Fig.15 a, b, c, and d) and vapor pressure deficit (Fig.15 e, f, g, and h) of the inflow air parcels to the inner-core along the latitude for Control, Dry, Saturate, and No LHF cases within the back-trajectory analysis datasets. In each panel, left to right direction is consistent with the air parcels' flow directions from south to north or from ocean to land. It is notable that clear decreasing trend exists in T_{air} along the trajectories towards north in general. Due to the decreasing T_{air}, vapor pressure deficit (Fig.15e-h) is pushed towards zero state within the moist PBL as airmass travels north. Only Dry case has more room for the evaporation in terms of the atmospheric vapor pressure deficit in the PBL. This means that the magnitude of LHF can be limited by the near-

saturation vapor pressure condition in the lower PBL regardless of the other major factors mentioned above.

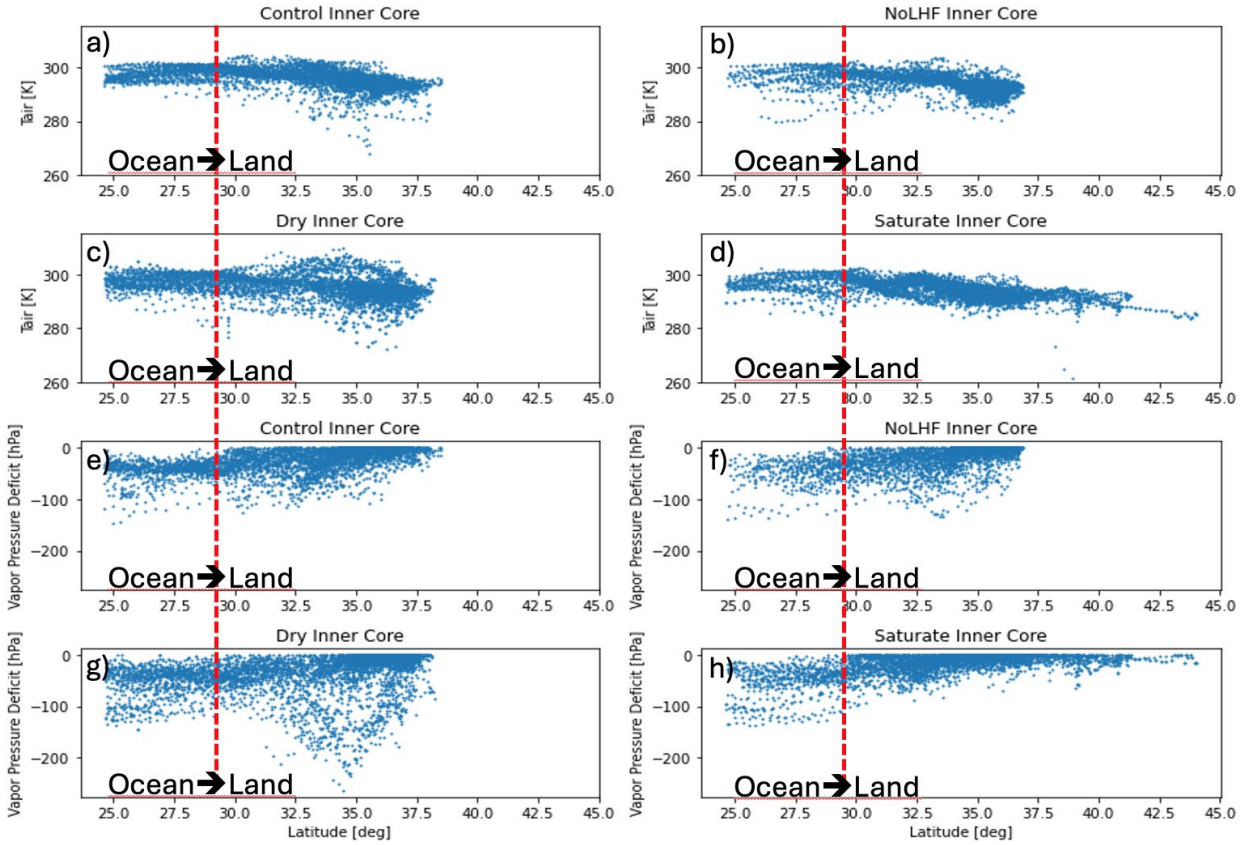

Figure 15. Scatter plots of T_{air} (a, b, c, and d) and vapor pressure deficit (Fig.15 e, f, g, and h) along the latitude in the back-trajectory dataset of Control, Dry, Saturate, and No LHF cases. The vertical dash lines indicate an approximate latitude of coastline in the datasets.

Although in-depth analysis is warranted for the three storms of the 21 named TCs in 2021 whether they are attributable to soil moisture anomalies, recall that their heavy precipitation was the common factor amongst them. Since most of the TCMIs occur in the form of TCs of low intensity as a tropical depression, their wind speed may not be destructive. However, tropical depressions can still pose a great threat with heavy rains to cause flooding as shown in Fig. 9. Due to the latitude-vapor pressure deficit relationship as suggested in Fig. 15, the chances of these heavy precipitation events can be increased if TCs could penetrate further north under a warming climate. Considering the current understanding of global trends of the warming air temperature that can be at least partially attributed to the anthropocene (e.g., human activities and urbanization in the coastal region), it is likely that the TCMI frequency may be increased in

the future due to these temperature and vapor pressure deficit effects (i.e., increased air temperature in the landfalling regions allows for greater evaporation from moist surfaces). Therefore, soil moisture and temperature conditions should be monitored throughout the entire landfalling domain both before and throughout the landfall and inland track (including both inner and outer core and background environment) of TCs to improve our prediction of the potential TCMI and associated heavy rainfall, wind, and flooding impacts. Further study is warranted for preparedness plans for landfalling TCs considering the continuum of soil wetness conditions.

Acknowledgements: This study was funded by NASA Modeling, Analysis, and Prediction (MAP) program (16-MAP16-013). NASA NCCS Discover and ADAPT cluster computers have been used for our LIS/NU-WRF model simulations, data analyses, and 3D visualizations.

Availability Statement: Authors are aware of the AMS data and software policies. Datasets and software used in the paper are archived and should be available upon requests.

Appendix

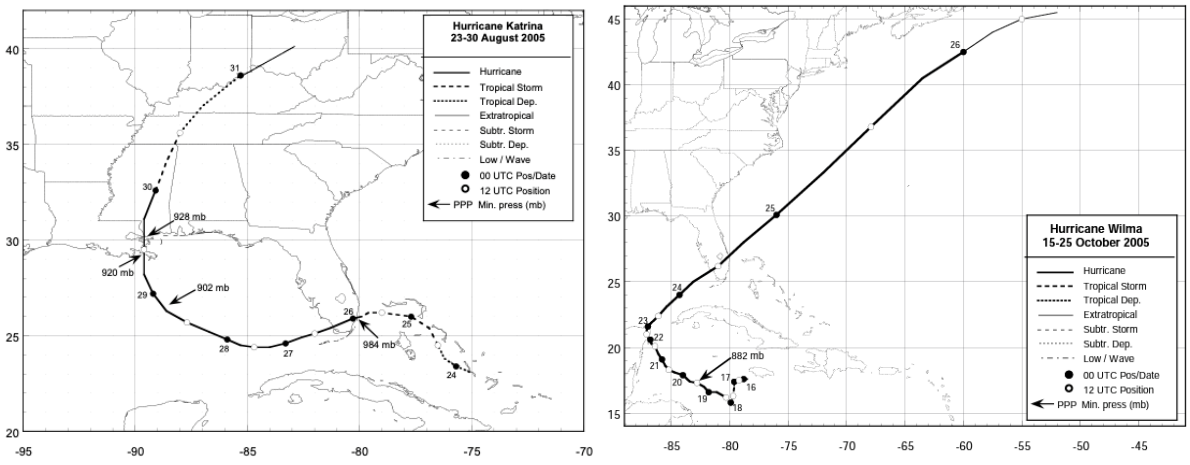

Figure A1. Best track positions for Hurricanes Katrina and Wilma in 2005. Images were obtained from National Hurricane Center Tropical Cyclone Report by Knabb et al. (2005) and by Pasch et al. (2006), respectively.

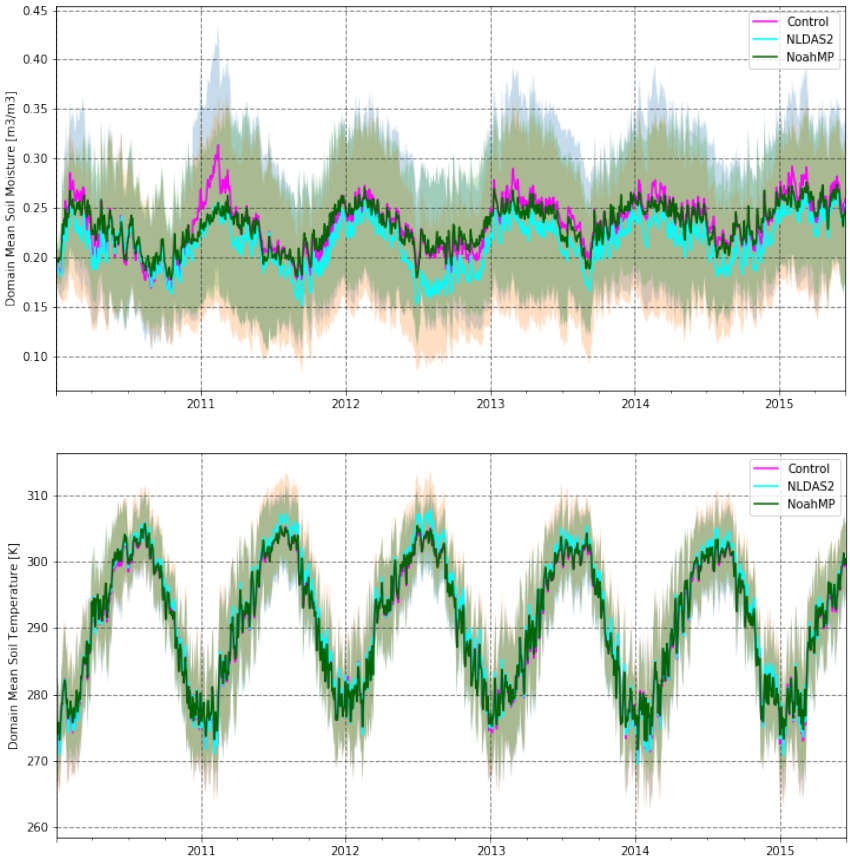

Figure A2. Temporal evolutions of domain average soil moisture and temperature of the LIS spinup runs (Control (i.e., GDAS), NLDAS2, and NoahMP) superimposed over the entire spectrum of their distributions over the model domain (light color).

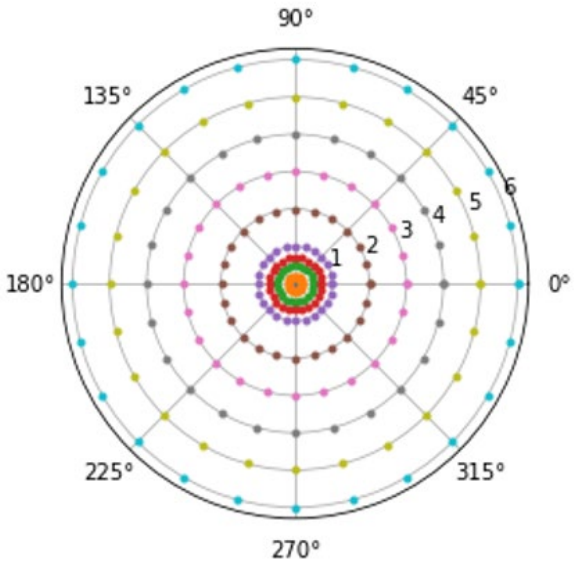

716

717 Figure A3. Schematic image of the spatial distribution of the trajectory seeds employed shown as
718 in colored dots at 25 azimuth angles in ten-radius distances from the center of the storm.1
719 through 6 indicate the outer radial rings in units of arc degree distances from the center.

720

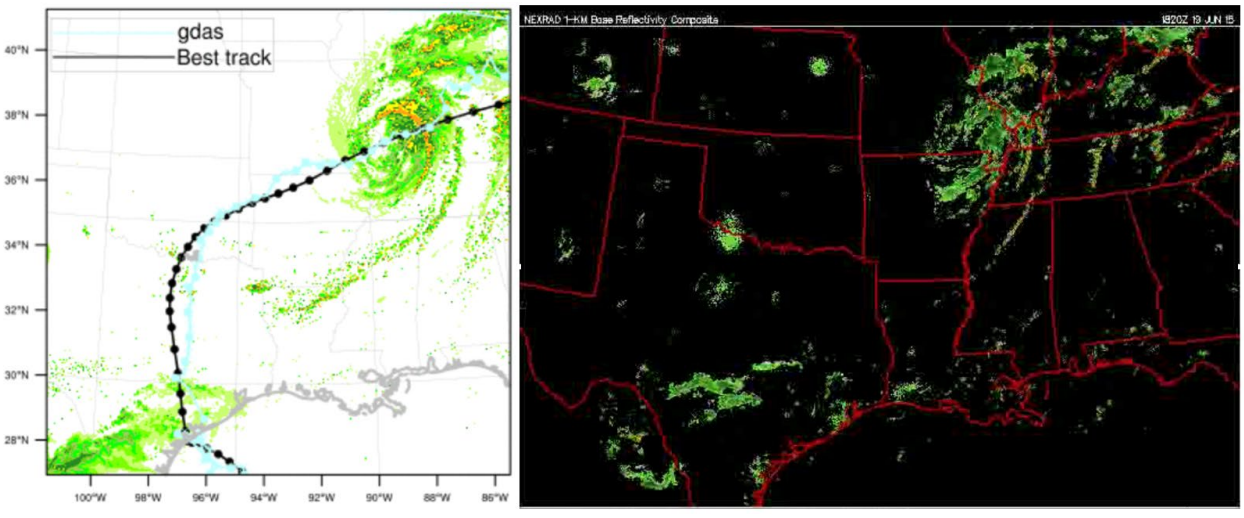

721

722 Figure A4. Composite radar reflectivities of pilot simulation case of the Control run (i.e., gdas
723 case; left) and NEXRAD imagery during the TCMI of the TS Bill (right).

724

725

References

Andersen, T. K., and J. M. Shepherd, 2013. A global spatiotemporal analysis of inland tropical cyclone maintenance or intensification. *Int. J. Climatol.*, **34**, 391–402, https://doi.org/10.1002/joc.3693.

Anthes, R. A., 1982. *Tropical Cyclones: Their Evolution, Structure and Effects*. Boston: American Meteorological Society.

Brauer, N. S., J. B. Basara, P. E. Kirstetter, R. A. Wakefield, C. R. Homeyer, J. Yoo, J. M. Shepherd, and J. A. Santanello Jr., 2021: The inland maintenance and reintensification of Tropical Storm Bill (2015). Part II: Precipitation microphysics. *J. Hydrometeor.*, **22**, 2695–2711, https://doi.org/10.1175/JHM-D-20-0151.1.

Dee, D. P., S. M. Uppala, A. J. Simmons, P. Berrisford, P. Poli, and co-authors, 2011. The ERA-interim reanalysis: configuration and performance of the data assimilation system. *QJR Meteorol. Soc.,* **137**, 553–597. doi:https://doi.org/10.1002/qj.828

Draxler, R. R., and G. D. Hess, 1998. An overview of the HYSPLIT_4 modeling system of trajectories, dispersion, and deposition. *Aust. Meteor. Mag.*, **47**, 295-308.

Emanuel, K. A., 1986. An air-sea interaction theory for tropical cyclones. Part 1: Steady-state maintenance, *J. Atmos. Sci.*, 43 (6), 585-605. DOI: https://doi.org/10.1175/1520-0469(1986)043<0585:AASITF>2.0.CO;2

Emanuel, K. E., J. Callaghan, and P. Otto, 2008. A hypothesis for the redevelopment of warm-core cyclones over northern Australia. *Mon. Wea. Rev.*, **136**, 3863-3872, https://doi.org/10.1175/2008MWR2409.1.

Evans C., R. S. Schumacher, and T. J. Galarneau, 2011. Sensitivity in the overland reintensification of Tropical Cyclone Erin (2007) to near-surface soil moisture characteristics. *Mon. Wea. Rev.*, **139**, 3848–3870, https://doi.org/10.1175/2011MWR3593.1.

Ferguson C. R., J. A. Santanello, and P. Gentine, 2016. Enhanced Soundings for Local Coupling Studies Field Campaign Report. Ed. by Robert Stafford, DOE ARM Climate Research Facility. DOE/SC-ARM-16-023.

754 Fleming, Z. L., P. S. Monks, and A. J. Manning, 2012. Review: Untangling the influence of air-
755 mass history in interpreting observed atmospheric composition. *Atmos. Res.*, **104–**
756 **105**, 1–39, doi:10.1016/j.atmosres.2011.09.009.
757 Frank, William M., 1977. The structure and energetics of the tropical cyclone I. Storm structure,
758 *Mon. Wea. Rev.*, **105**, 1119-1135. DOI: https://doi.org/10.1175/1520-
759 0493(1977)105<1119:TSAEOT>2.0.CO;2
760 Gopalakrishnan, S., Srinavas, C. V., & Bhatia, K., 2016. The hurricane boundary layer. In U. C.
761 Mohanty & S. G. Gopalakrishnan (Eds.), *Advanced numerical modeling and data*
762 *assimilation techniques for tropical cyclone predictions* (pp. 589–626). Netherlands:
763 Springer. Retrieved from https://www.springer.com/gp/book/97894
764 Gray, W. M., 1975. Tropical cyclone genesis. Dept. of Atmos. Sci. Paper No. 234, Colo. State
765 Univ., Ft. Collins, CO, 121 pp.
766 Hall, T. M., and J. P. Kossin, 2019. Hurricane stalling along the North American coast and
767 implications for rainfall. *NPJ Clim. Atmos. Sci.*, **2**, 17, doi:10.1038/s41612-019-0074-
768 8.
769 Hart, R. E. and J. L. Evans, 2001. A Climatology of the Extratropical Transition of Atlantic
770 Tropical Cyclones, *J. Climate*, **14**, 546-565. https://doi.org/10.1175/1520-
771 0442(2001)014<0546:ACOTET>2.0.CO;2
772 Kaplan, J. and M. DeMaria, 1995. A simple empirical model for predicting the decay of tropical
773 cyclone winds after landfall. *J. of Appl. Meteo*., **34**, 2499-2512.
774 Kim, J., B. Guan, D. E. Waliser, R. D. Ferraro, J. Case, T. Iguchi, E. Kemp, W. Putman, W.
775 Wang, D. Wu, and B. Tian: *Winter precipitation characteristics in western US related*
776 *to atmospheric river landfalls: observations and model evaluations*, Climate
777 Dynamics, 50, 231-248. DOI: 10.1007/s00382-017-3601-5.
778 Knapp, K. R., M. C. Kruk, D. H. Levinson, H. J. Diamond, and C. J. Neumann, 2010. The
779 international best track archive for climate stewardship (IBTrACS). *Bull. Amer.*
780 *Meteor. Soc.*, **91** (3), 363-376. DOI: https://doi.org/10.1175/2009BAMS2755.1

781 Knapp, K. R., M. C. Kruk, D. H. Levinson, H. J. Diamond, and C. J. Neumann, 2010. The
782 International Best Track Archive for Climate Stewardship (IBTrACS): Unifying

783 tropical cyclone best track data. *Bull. Amer. Meteor. Soc.*, **91**, 363-
784 376. doi:10.1175/2009BAMS2755.1

785 Kumar, S.V., C. D. Peters-Lidard, Y. Tian, P. R. Houser, J. Geiger, S. Olden, L. Lighty, J. L.
786 Eastman, B. Doty, P. Dirmeyer, J. Adams, K. Mitchell, E. F. Wood, and J. Sheffield,
787 2006. Land Information System - An interoperable framework for high resolution land
788 surface modeling. *Environ. Modeling & Software*, **21**, 1402-
789 1415, doi:10.1016/j.envsoft.2005.07.004
790 Lawston, Patricia M., J. A. Santanello, B. Hanson, and K. Arsensault, 2020. Impacts of Irrigation
791 on Summertime Temperatures in the Pacific Northwest, *Earth Interactions*, **24** (1),
792 1087-3562.
793 Li, Z., A. Tiwari, X. Sui, J. Garrison, F. Marks, and D. Niyogi, 2023. Studying Brown Ocean re-
794 intensification of Hurricane Florence using CYGNSS and SMAP soil moisture data
795 and a numerical weather model. *Geophys. Res. Lett.*, **50**, e2023GL105102. https://doi.
796 org/10.1029/2023GL105102
797 Messmer, M., C. C. Raible, and J. J. Gomez-Navarro, 2020. Impact of climate change on the
798 climatology of Vb cyclones, *Tellus A*, **72**, 1724021,
799 https://doi.org/10.1080/16000870.2020.1724021.

800 Miller, B. I., 1964: A study on the filling of Hurricane Donna (1960) over land. *Mon. Wea. Rev.*,
801 **92**, 389-406.

802 Montgomery, M. T., M. M. Bell, S. D. Aberson and M. L. Black, 2006. New insights into the
803 Physics of Intense storms. Part I: Mean Vortex Structure and Maximum Intensity
804 Estimates. *Bull. Amer. Meteor. Soc.*, **87**, 1335-1347.

805 Nair, U.S., E. Rappin, E. Foshee, *et al., 2019.* Influence of Land Cover and Soil Moisture based
806 Brown Ocean Effect on an Extreme Rainfall Event from a Louisiana Gulf Coast
807 Tropical System. *Sci Rep.* **9**, 17136. https://doi.org/10.1038/s41598-019-53031-6

808 Ooyama, K., 1969. Numerical simulation of the life cycle of tropical cyclones. *J. Atmos. Sci*., **26**,
809 3-40.

Peters-Lidard, C.D., and Coauthors, 2015: Integrated modeling of aerosol, cloud, precipitation and land processes at satellite-resolved scales. *Environ. Modell. Software*, **67**, 149–159, https://doi.org/10.1016/j.envsoft.2015.01.007.

Peters-Lidard, C.D., P.R. Houser, Y. Tian, S.V. Kumar, J. Geiger, S. Olden, L. Lighty, B. Doty, P. Dirmeyer, J. Adams, K. Mitchell, E.F. Wood, and J. Sheffield, 2007. High-performance Earth system modeling with NASA/GSFC's Land Information System. *Innovations in Systems and Software Engineering*, **3**(3), 157-165, doi:10.1007/s11334-007-0028-x

Peters-Lidard, C.D., P.R. Houser, Y. Tian, S.V. Kumar, J. Geiger, S. Olden, L. Lighty, B. Doty, P. Dirmeyer, J. Adams, K. Mitchell, E.F. Wood, and J. Sheffield, 2007. High-performance Earth system modeling with NASA/GSFC's Land Information System. *Innovations in Systems and Software Engineering*, **3**(3), 157-165, doi:10.1007/s11334-007-0028-x

Rosenthal, S. L., 1971. The response of a tropical cyclone model to variations in boundary layer parameters, initial conditions, lateral boundary conditions, and domain size. *Mon. Wea. Rev.*, **99**, 767-777.

Santanello, J. A., 2011a. Results from Local Land-Atmosphere Coupling (LoCo) Project *GEWEX Newsletter,* **21 (4)**: 7-9

Santanello, J. A., C. D. Peters-Lidard, and S. V. Kumar, 2011b. Diagnosing the Sensitivity of Local Land–Atmosphere Coupling via the Soil Moisture–Boundary Layer Interaction *J. Hydrometeor* **12 (5)**: 766-786 [10.1175/JHM-D-10-05014.1]

Santanello, J. A., C. D. Peters-Lidard, S. V. Kumar, C. Alonge, And W.-K. Tao, 2009. A Modeling and Observational Framework for Diagnosing Local Land–Atmosphere Coupling on Diurnal Time Scales, *J. Hydrometeor.*, **10**, 577-599, DOI: 10.1175/2009JHM1066.1.

Santanello, J. A., P. A. Dirmeyer, C. R. Ferguson, et al. K. L. Findell, A. B. Tawfik, A. Berg, M. Ek, P. Gentine, B. P. Guillod, C. van Heerwaarden, J. Roundy, and V. Wulfmeyer, 2018. Land-Atmosphere Interactions: The LoCo Perspective, *Bull. Amer. Meteor. Soc.*, **99 (June)**: 1253-1272 [10.1175/bams-d-17-0001.1]

Santanello, J. A., P. Lawston, S. Kumar, and E. Dennis, 2019: Understanding the impacts of soil moisture initial conditions on NWP in the context of land–atmosphere coupling. *J. Hydrometeor.*, **20**, 793–819, https://doi.org/10.1175/JHM-D-18-0186.1.

Santanello, J. A., S. V. Kumar, C. D. Peters-Lidard, and P. M. Lawston, 2016. Impact of Soil Moisture Assimilation on Land Surface Model Spinup and Coupled Land-Atmosphere Prediction *J. Hydrometeor.,* **17,** 517-540 [10.1175/jhm-d-15-0072.1].

Schroeder, A., J. Basara, J. M. Shepherd, and S. Nelson, 2016: Insights into Atmospheric Contributors to Urban Flash Flooding across the United States Using an Analysis of Rawinsonde Data and Associated Calculated Parameters. *J. Appl. Meteor. Climatol.*, 55, 313-323, DOI: https://doi.org/10.1175/JAMC-D-14-0232.1.

Shi, J. J., S. A. Braun, Z. Tao, and T. Matsui: Modeling of the influence of Saharan dust and other Aerosols on Hurricane Nadine (2012) During the NASA Hurricane and Severe Storm Sentinel (HS3) investigation. *Mon. Wea. Rev.*, 149, 3541-3562, DOI: 10.1175/MWR-D-20-0344.1, 2021

Sodemann, H., C. Schwierz, & H. Wernli, 2008. Interannual variability of Greenland winter precipitation sources: Lagrangian moisture diagnostic and North Atlantic Oscillation influence. *J. Geophys. Res-Atmos*., **113**, D03107.

Stein, A.F., R.R. Draxler, G.D. Rolph, B.J.B. Stunder, M.D. Cohen, and F. Ngan, 2015. NOAA's HYSPLIT atmospheric transport and dispersion modeling system, *Bull. Amer. Meteor. Soc*., **96**, 2059-2077, http://dx.doi.org/10.1175/BAMS-D-14-00110.1

Tao, Z., M. Chin, M. Gao, T. Kucsera, D. Kim, H. Bian, J. Kurokawa, Y. Wang, Z. Liu, G. R. Carmichael, Z. Wang, and H. Akimoto, Evaluation of NU-WRF performance on air quality simulation under various model resolutions – an investigation within framework of MICS-Asia Phase III. Atmospheric Chemistry & Physics, 20: 2319-2339, https://doi.org/10.5194/acp-20-2319-2020, 2020.

Tao, Z., S.A. Braun, J.J. Shi, M. Chin, D. Kim, T. Matsui, and C.D. Peters-Lidard, *Microphysics and radiation effect of dust on Saharan air layer: An HS3 case study*, Mon. Wea. Rev., 146, 1813-1835, doi:10.1175/MWR-D-17-0279.1, 2018.

Tuleya, R. E., 1994. Tropical storm development and decay: Sensitivity to surface boundary conditions. *Mon. Wea. Rev.*, **122**, 291-304.

869 Tuleya, R. E., M. A. Bender, and Y. Kurihara, 1984. A simulation study of the landfall of
870 tropical cyclones using a movable nested-mesh model. *Mon. Wea. Rev.*, **112**, 124-136.

871 Visualization & Analysis Systems Technologies. (2023) Visualization and Analysis Platform for
872 Ocean, Atmosphere, and Solar Researchers (VAPOR version 3.8.0) [Software].
873 Boulder, CO: UCAR/NCAR – Computational and Information System
874 Lab. doi:10.5281/zenodo.7779648

875 Vose, R. S., S. Applequist, M. Squires, I. Durre, M. J. Menne, C. N. Jr. Williams, C. Fenimore,
876 K. Gleason, and D. Arndt, 2014. NOAA Monthly U.S. Climate Gridded Dataset
877 (NClimGrid), Version 1. NOAA National Centers for Environmental Information.
878 DOI:10.7289/V5SX6B56.

879 Wakefield, R. A., J. B. Basara, J. M. Shepherd, Noah Brauer, J. C. Furtado, J. A. Santanello Jr.,
880 and R. Edwards, 2021. The inland maintenance and reintensification of Tropical
881 Storm Bill (2015). Part I: Contributions of the brown ocean effect. *J.*
882 *Hydrometeor.*, **22**, 2675–2693, https://doi.org/10.1175/JHM-D-20-0150.1.
883 Wuertz, D., J. Lawrimore, and B. Korzeniewski, 2018. Cooperative Observer Program (COOP)
884 Hourly Precipitation Data (HPD), Version 2.0. NOAA National Centers for
885 Environmental Information. doi:10.25921/p7j8-2170.
886 Yerramilli et al., 2012. An integrated WRF/HYSPLIT modeling approach for the assessment of
887 PM2.5 source regions over the Mississippi Gulf Coast region, *Air Qual. Atmos.*
888 *Health*., **5**(4): 401–412. doi: 10.1007/s11869-010-0132-1
889 Yoo, J., J. Santanello, M. Shepherd, *et al*., 2020. Quantification of the Land Surface and Brown
890 Ocean Influence on Tropical Cyclone Intensification over Land. *J. Hydrometeor.,* **21**,
891 6, 1171-1192.
892 Zhu, Yi-Jie et al. "Hurricane Ida (2021): Rapid Intensification Followed by Slow Inland Decay"
893 vol. 103, no. 10, 2022, https://doi.org/10.1175/bams-d-21-0240.1